**W-AM-SymI-1**

SIMPLE MODELS OF PROTEIN FOLDING. ((K.A. Dill)) Univ. of California, San Francisco.

**W-AM-SymI-2**

A BINARY CODE FOR PROTEIN DESIGN: NOVEL PROTEINS BY THE DOZEN (Michael H. Hecht, Satwik Kamtekar, Jarad Schiffer, Huayu Xiong, and Jennifer Babik) Dept. of Chemistry and Dept. of Molecular Biology. Princeton University, Princeton, NJ 08544-1009.

A general strategy will be presented for the design of proteins *de novo*. The strategy assumes that it is *sufficient* to design sequences capable of burying hydrophobic surface area while simultaneously forming abundant secondary structure. Specific inter-residue packing is not specified a priori. Thus, sequence *locations* of hydrophobic and hydrophilic residues are specified explicitly, but the precise *identities* of the hydrophobic (or hydrophilic) residues are not be constrained and can be varied extensively. We have experimentally tested this strategy by constructing a large collection of sequences that satisfy these criteria and are designed to fold into 4-helix bundle proteins. The collection was assembled by constructing a degenerate family of synthetic genes. Each member of this family encodes a different amino acid sequence, but they all encode sequences sharing the same pattern of polar and non-polar residues. The sequence degeneracy is made possible by using degenerate codons: Wherever a non-polar residue is required, the degenerate codon NTN is used (giving Phe, Leu, Ile, Met, or Val); wherever a polar residue is required, the degenerate codon NAN is used (giving Glu, Gln, Asp, Asn, Lys, or His). We have produced a large collection of novel proteins fitting this pattern. Their characterization indicates that most of them fold into compact α-helical structures. Thus a simple binary code of polar and non-polar residues arranged in the appropriate order can be sufficient for *de novo* protein design.

**W-AM-SymI-3**

DESIGN OF METALLOPROTEINS AND TUBULAR PROTEINS. ((R. Ghadiri)) Scripps Research Inst.

**W-AM-SymI-4**

DE NOVO DESIGN OF HELICAL PROTEINS ((W. DEGRADO)) DuPont Merck Pharmaceut. Co.

## TRANSPORTERS IN THEIR GLORY

**W-AM-A1**

**U-SHAPED DEPENDENCE OF MEMBRANE POTENTIAL ON $Na^+$-$K^+$ PUMP ACTIVITY.** ((A.Y. Kabakov)) Institute of Developmental Biology, Moscow, Russia 117808. (Present address: Department of Physiology, UTSW Medical Center at Dallas, Dallas, Texas 75235-9040)

A U-shaped dependence of the resting potential (RP) on $Na^+$-$K^+$ pump activity was theoretically grounded (J. Theor. Biol., 169, 51-64) and experimentally confirmed. When the pump activity is so high that $(E_K[K^+]_i + E_{Na}[Na^+]_i)/([K^+]_i + [Na^+]_i) < RP$, where $E_K$ and $E_{Na}$ are Nernst equilibrium potentials for $K^+$ and $Na^+$ ions, $[K^+]_i$ and $[Na^+]_i$ are their intracellular concentrations, then activation of the $Na^+$-$K^+$ pump results in depolarization. The energy of ATP hydrolysis is sufficient to transfer the cardiac $Na^+$-$K^+$ pump into the depolarizing state.

The $Na^+$-$K^+$ pump of frog ventricular cardiomyocytes is in the depolarizing state. Therefore application of nanomolar concentrations of ouabain results in hyperpolarization, that confirm the U-shaped form of the dependence.

**W-AM-A2**

PHOTOAFFINITY LABELING THE ACTIVE SITE OF THE $Na^+/K^+$-ATPase WITH 4-AZIDO-2-NITROPHENYLPHOSPHATE. ((Chinh M. Tran and Robert A. Farley)) U. Southern California, School of Medicine, Dept. of Physiology & Biophysics, Los Angeles CA 90033.

4-Azido-2-nitrophenylphosphate (ANPP), a photoreactive analogue of *p*-nitrophenylphosphate (pNPP) was synthesized. ANPP was hydrolyzed by $Na^+/K^+$-ATPase with a Vmax of 0.36 μmol/mg/min, and an apparent Km of about 0.98 mM. The Km for pNPP was 1.7 mM. ANPP acts as a competitive inhibitor of pNPP hydrolysis with a Ki of about 0.37 mM. After photolysis with UV light (310 nm, 350 $\mu W/cm^2$, 30 min), ANPP inhibited both ATPase (k=0.067/min/M) and pNPPase activity (k=0.044/min/M) of the $Na^+/K^+$-ATPase in a concentration-dependent manner. Inhibition was partially prevented by 0.2 mM $Na_2$-ATP or by excluding $Mg^{2+}$ from the photolysis buffer. Photolysis with [$^{32}$P]-ANPP labeled only the α subunit of the $Na^+/K^+$-ATPase and the amount of labeling was substantially reduced by the presence of 0.2 mM $Na_2$-ATP, or in the absence of $Mg^{2+}$. The stoichiometry of labeling reached a maximum of about 1 nmol/mg at 100% inhibition of $Mg^{2+}$-sensitive activity. Limited proteolytic digestion showed labeling sites on non-overlapping peptides derived from the α subunit of $Na^+/K^+$-ATPase. HPLC analysis of an exhaustive tryptic digest of $^{32}$P-ANPP-labeled $Na^+/K^+$-ATPase identified two radiolabeled tryptic peptides, one from Met-379 to Lys-406, and the second from Ala-655 to Lys-676. The first peptide is close to the Asp-369 that is phosphorylated by ATP, and the second peptide is a peptide suggested to be labeled by FSBA. Amino acids corresponding to Asn-398 and Pro-668 were missing from the sequences, and may be located in the active site of the Na,K-ATPase. (NIH GM28673)

**W-AM-A3**

MECHANISM OF ACTION OF GENERAL ANESTHETICS ON PM $Ca^{2+}$-ATPase IN ERYTHROCYTE AND BRAIN CELLS. ((D. Kosk-Kosicka, M. Lopez, I. Fomitcheva, G. Roszczynska)), Johns Hopkins University, School of Medicine, Dep. of Anesthesiology, Baltimore, MD 21287.

We have demonstrated that halothane inhibits $Ca^{2+}$-ATPase activity of the plasma membranes (PM) of erythrocytes, brain capillaries, and synaptosomal membranes preparations. As the inhibition occurs at clinically relevant concentrations it is plausible that impairment of this enzyme, instrumental in maintaining $Ca^{2+}$ homeostasis, may be related to anesthetic effects occuring in clinical anesthesia. Thus, it is compelling to explain the mechanism of $Ca^{2+}$-ATPase inhibition by anesthetics. We have shown that halothane and several other volatile anesthetics (VA) affect $Ca^{2+}$ binding that initiates the catalytic cycle of the $Ca^{2+}$-ATPase. VA do not decrease $Ca^{2+}$ binding to SR $Ca^{2+}$-ATPase, as shown in parallel studies, which supports functional importance of VA action selectively on PM $Ca^{2+}$-ATPase. We have also evaluated the effects of other groups of general anesthetics, including barbiturates (in clinical use) and alkanols (used as model anesthetics). We conclude that all of them inhibit PM $Ca^{2+}$-ATPase activity; however there are apparent differences in their mechanisms of action. VA are the most potent with the fastest onset of inhibition. Barbiturates and alkanols on the other hand differentiate between the CaM-dependent and CaM-independent $Ca^{2+}$-ATPase species, inhibiting the later more effectively. In addition alkanols and to a lesser degree barbiturates, decrease $Ca^{2+}$ affinity of the enzyme. (NIH 447130 & AHA 92010190)

**W-AM-A4**

**CALCIUM PUMP KINETICS IN SINGLE ERYTHROCYTE GHOSTS DETERMINED BY MICROPHOTOLYSIS AND CONFOCAL IMAGING.** ((U.Kubitscheck*, L.Pratsch*, H.Passow# and R.Peters*)) *Institut für Medizinische Physik und Biophysik der Universität, Münster, and #Max-Planck-Institut für Biophysik, Frankfurt, Germany

The activity of the plasma membrane calcium pump was measured by microphotolysis in a confocal microscope. Human erythrocyte ghosts were loaded with a fluorescent calcium indicator and either a) caged calcium and ATP, or b) caged ATP and calcium. In a suitably modified laser scanning microscope (Leica) calcium or ATP were released by a short UV pulse and the time-dependent fluorescence intensity of the calcium indicator followed by repetitive confocal imaging. The fluorescence intensity was converted into calcium concentration which in turn was used to derive the kinetic parameters of the calcium pump. Km- and Vmax-values derived in this manner were 24 ± 14 µM and 1.0 ± 0.6 µM/s for condition a), and 4 ± 3 µM and 1.0 ± 0.6 µM/s for condition b). The difference between a) and b) is presumably due to the action of calmodulin which is inactive in a). Optical single-cell and single-channel flux measurements open new possibilities for characterizing membrane transport proteins (cf. EMBO J. 9 (1990) 2447 - 2451). (Supported by the Deutsche Forschungsgemeinschaft)

**W-AM-A5**

**USING RAPID PERFUSION TO STUDY THE CURRENT ASSOCIATED WITH SODIUM BINDING TO THE GABA TRANSPORTER GAT1.**

((Mager Sela, Gilmor I. Keshet*, Baruch I. Kanner*, Norman Davidson and Henry A. Lester)) Caltech, Division of Biology Pasadena, CA 91125. *Hebrew University, Medical school, Jerusalem, Israel 91010.

We used voltage clamp and fast perfusion to study the sodium interaction with the mammalian GABA transporter GAT1 expressed in *Xenopus* oocytes. Oocytes were clamped at -80 mV with two electrode voltage clamp. Solution was exchange in 1-2 sec. When the perfused solution was changed from $Na^+$ ringer to $Na^+$ free ringer (with $NMDG^+$ or $Li^+$ as substitute) a transient outward current developed. A similar but opposite transient inward current developed when the perfusion was changed back to $Na^+$ ringer. The transient current decreased when oocytes were held at a less negative potential. The integral of the transient current was similar to the integral of the transient currentthat developed in response to voltage jump to a positive potential (see Mager at el, 1993, Neuron 10:177-188). We conclude that these transient currents reflect charge movement associated with $Na^+$ binding and dissociation. Support: NIH, MDA, BSF, L. Deutsch Fnd.

**W-AM-A6**

CURRENT FLUCTATIONS IN NOREPINEPHRINE TRANSPORTERS. ((L. J. DeFelice, A. Galli, R. D. Blakely)) Anatomy & Cell Biology, Emory University School of Medicine, Atlanta GA 30322.

To study the uptake mechanisms of neurotransmitter transporters, we have measured current fluctuations in 293 cells stably-transfected with a cloned human norepinephrine (NE) transporters (hNET). Radiolabeled flux assays show that these cells transport NE and guanethidine (GU). In physiological solutions under whole-cell voltage clamp at 37 °C, NE or GU generate a mean inward current and an increase in current fluctuations at negative voltages. The $K_m$ for the mean current is 0.6 uM for NE and 1.1 uM for GU at -120 mV. The antidepressant desipramine (DS) inhibits the mean current with a $K_i$ of 0.05 uM. DS also suppresses the induced fluctuations. At -120 mV the maximum induced currents range from -50 to -120 pA. The control variance (no GU or NE) is typically 16 $pA^2$ at -120 mV. In 15 uM GU the variance increases to 28 $pA^2$. After adding 2 uM DS the variance decreases to 12 $pA^2$ (5000 Hz bandwidth). Parental cells have no NE- or GU-induced current fluctuations. The ratio of the change in variance to the change in the mean is typically 0.25 pA. This ratio is independent of the concentration of GU or NE between 0 and 20 uM. Mammalian cells stably-transfected with cloned transporters are a useful model in which to study the mechanism of uptake. We will present a stochastic scheme of NE transport based on the mean and the variance of the substrate-induced currents in this model system.

**W-AM-A7**

LONG-RANGE PROTON TRANSFER ALONG THE MEMBRANE SURFACE IS FASTER THAN PROTON EXCHANGE WITH THE BULK WATER PHASE. ((N.A. Dencher, J. Heberle§, D. Oesterhelt#, J. Riesle# and G. Thiedemann*)) Inst. Biochemie, Techn. Hochschule, Petersenstr. 22, D-64287 Darmstadt; Germany; §IBI-2, KFA, D-52425 Jülich; #MPI Biochemie, D-82152 Martinsried; *BENSC, HMI, D-14109 Berlin.

To unravel the elementary proton transfer reactions powering complex chemiosmotic systems, we study the well characterized purple membrane (PM). With bacteriorhodopsin (BR), a light-driven proton pump, both vectorial proton transfer steps across the membrane at almost atomic level and along the surface can be examined. $H^+$-transfer processes from the active centre of BR to the extracellular side and from there along the membrane-water interphase to the cytoplasmatic BR side are kinetically and spatially resolved by flash absorption spectroscopy in combination with optical pH-indicators bound selectively to both membrane surfaces. All pumped protons are diffusing laterally along the membrane surface for long distances (several thousand Å) before equilibrating into the aqueous bulk phase. However, $H^+$-ions move slower (diffusion coefficient $D_{app} = 9.6 * 10^{-7}$ $cm^2/s$, including reactions at the PM rim) than in the aqueous bulk phase ($D = 9.3 * 10^{-5}$ $cm^2/s$). The anisotropic long-range translational diffusion of water molecules at the PM surface ($D_s = 4.4 * 10^{-6}$ $cm^2/s$; Lechner et al., Solid State Ionics 70/71, 296-304, 1994) is 5-times faster than the measured $H^+$-transfer rate along the surface. Therefore, diffusing water molecules can act as vehicles. $H^+$-transfer along a membrane surface could significantly contribute to, or even dominate, chemiosmotic energy coupling.

**W-AM-A8**

PURIFICATION AND SUBSTRATE SPECIFICITY OF THE RED CELL AMINOPHOSPHOLIPID FLIPPASE. ((David Daleke, Jill Lyles, Edward Nernergut, and Michael Zimmerman)) Dept. of Chem., Indiana University, Bloomington, IN 47405.

Transmembrane aminophospholipid asymmetry is maintained by a PS- and PE-specific, Mg-ATP-dependent transporter (flippase) that is sensitive to sulfhydryl reagents, vanadate and calcium. A candidate aminophospholipid flippase has been purified from human erythrocytes that possesses many enzymatic characteristics similar to that of the flippase. The detergent solubilized ATPase is inactive in the absence of added phospholipids and is maximally stimulated by PS. PE and negatively charged lipids afford partial activation, but net neutral lipids do not support ATPase activity. This specificity is reminiscent of that demonstrated by the flippase; PS is the optimal substrate for the flippase, while PE is transported less efficiently. The essential structural features of PS required for activation of the ATPase or transport by the flippase were studied using synthetic PS analogs. The amine group is required by both enzymes; phosphatidylhydroxypropionate did not activate the ATPase, nor was it transported by intact erythrocytes. *N*-methylation had no effect on transport and only partially reduced the activation of the ATPase. The carboxyl group is not essential, but is required for maximal activity; PE activates the ATPase 4-fold less than PS and is transported at a rate 10-fold slower. The activity of both enzymes is dependent on the presence of a charged phosphate; replacing the phosphate with an uncharged, isosteric sulfonate abolishes both transport and ATPase stimulation. Most significant, however, is the sensitivity of these enzymes to PS stereochemistry. While the stereoconfiguration of the serine headgroup is unimportant, both enzymes are selectively stimulated by the naturally occurring *sn*-1,2 glycerol isomer and not the *sn*-2,3 isomers. These data indicate that both the flippase and the partially purified ATPase show an extreme specificity for the structure of the lipid substrate that involves several recognition elements including the headgroup, phosphate and glycerol backbone. The striking similarity of the lipid specificity of both enzymes supports the proposition that the ATPase and the flippase may be identical.

**W-AM-A9** *(See Th-Pos440)*

W-AM-B1

**LOCATION OF THE α-BUNGAROTOXIN BINDING SITES ON THE NICOTINIC ACETYLCHOLINE RECEPTOR SUPERSTRUCTURE: A LOW ANGLE X-RAY DIFFRACTION STUDY.** ((Howard S. Young, Victor Skita, Leo G. Herbette)) Biomolecular Structure Analysis Center, University of Connecticut Health Center, Farmington, CT 06030-2017

A profile structure at 14Å resolution has been presented for the nicotinic acetylcholine receptor (AChR) membrane from *Torpedo californica* using the technique of low angle x-ray diffraction (Young et al. 1994, Biophys. J. 66:A7). Analysis of the meridional diffraction data indicated a 452Å ± 5Å (n = 21) lattice spacing between stacked vesicle membrane pairs with an average resolution of approximately 8Å. In the plane of the membrane, the AChR molecules were organized in a hexagonal lattice with a nearest neighbor distance of 80Å ± 1Å. Interpretation of the electron density profile gave a cytoplasmic extension of 35Å for the AChR and associated 43kDa protein, a lipid bilayer thickness of 43Å (phospholipid headgroup-to-headgroup spacing), and a synaptic extension of 90Å. A cylindrically averaged model for the AChR, derived from the profile structure, bears a striking resemblance to the three-dimensional reconstructions from cryo-electron microscopy of tubular crystals (Unwin, 1993, J. Mol. Biol. 229:1101-1124). In the presence of α-bungarotoxin, the quality of the diffraction data and the meridional lattice spacing were unchanged. In the plane of the membrane, the nearest neighbor distance between hexagonally packed AChRs increased to 85Å ± 1Å in the presence of toxin. Profile structures calculated in the presence and absence of α-bungarotoxin indicated a location for the toxin binding sites 26Å above the hydrocarbon core/water interface of the membrane. Additional changes in the profile structure, restricted to the synaptic and transmembrane domains of the AChR, were attributed to conformational changes in the AChR upon α-bungarotoxin binding. [Supported by: Marion Merrell Dow, Cincinnati, OH; Univ. of Conn. Health Ctr., Farmington, CT; NIH RR01633]

W-AM-B2

MECHANISM OF INHIBITION OF THE MUSCLE NICOTINIC ACETYLCHOLINE RECEPTOR (nAChR) INVESTIGATED BY A LASER-PULSE PHOTOLYSIS TECHNIQUE. ((L. Niu, C. Grewer, *L.G. Abood and G.P. Hess)) Section of Biochemistry, Molecular and Cell Biology, Cornell University, Ithaca, NY 14853-2703 (Spon. by L.M. Nowak)

Inhibition of the nAChR by procaine, a local anesthetic, cocaine, a powerful drug of abuse, and MK-801, an anticonvulsant compound and a potent inhibitor of the NMDA receptor, has been investigated. A laser-pulse photolysis technique with a 100-μs time resolution, in combination with a cell-flow technique with a 10-ms time resolution, has been used to determine the effects of these inhibitors on (i) the rate constant of channel opening, (ii) the rate constant of channel closing, (iii) the apparent dissociation constants of the inhibitor from the closed- and the open-channel forms. (iv) The rates with which the inhibitors bind to the closed- and open-channel forms can be estimated. These measurements allow one to discriminate between two mechanisms for the inhibition reaction: (i) the inhibitor binds in the open receptor-channel and blocks it, or (ii) the inhibitor binds to a regulatory site on the closed-channel form. The results obtained with all three inhibitors exclude a mechanism in which receptor inhibition occurs solely by the inhibitor binding to the open-channel form of the receptor.

This work was supported by grants from the National Institutes of Health. CG is grateful for a Feodor Lynen Fellowship from the A. v. Humboldt Foundation.

*Department of Pharmacology, University of Rochester Medical School, Rochester, NY.

W-AM-B3

**HYDROPHOBIC MUTATIONS IN THE M2 DOMAIN OF NICOTINIC ACH RECEPTORS MODULATE N-ALCOHOL BLOCKING POTENCIES.** ((Stuart A. Forman, Keith W. Miller & Gary Yellen)) Depts. of Anesthesia and Neurobiology, Massachusetts General Hospital, Boston, MA 02114.

General anesthetics may inhibit synaptic membrane proteins by perturbing surrounding lipids or by direct interactions with protein sites. Anesthetic n-alcohols inhibit the nAChR with features that suggest a channel block mechanism. Local anesthetic channel blockers have been shown to bind to the 6' and 10' loci (1' at the cytoplasmic surface) on the second transmembrane (M2) domains of nAChR subunits by site-directed mutagenesis (Charnet et al, 1990; *Neuron* 2, 89-95). We tested the hypothesis that alcohols bind at a similar site. Mutant mouse muscle nAChR subunits with increased side-chain hydrophobicity at the 10' and 6' loci in M2 were constructed using site-directed mutagenesis. ACh and alcohol effects were assessed by fast perfusion patch-clamp electrophysiology in *Xenopus* oocytes expressing wild type and mutant nAChRs. We show that: 1) Octanol preferentially inhibits the open channel state of both wild-type nAChR and a mutant receptor, α-S10'I. 2) Graded increases in the hydrophobicity at the 10' locus on the α subunit (S→V, I, or F) produce increases in n-alcohol inhibitory potencies. Hydrophobicity mutations at the 10' locus on the β subunit are additive with those on α, producing over a 10-fold decrease in hexanol's $IC_{50}$ for the α-S10'I & β-T10'I mutant. 3) Similar mutations at the 6' loci on α and β subunits cause no change in n-alcohol potencies. The data support a mechanism where hydrophobic forces dominate general anesthetic drug binding at a discrete inhibitory region within the nAChR ion pore.

(Supported by the Foundation for Anesthesia Education and Research with a grant from Marquette Electronics).

W-AM-B4

AMINO ACID SUBSTITUTIONS AT THE LIPID-PROTEIN INTERFACE OF THE ACETYLCHOLINE RECEPTOR MAY PLAY A KEY ROLE IN CHANNEL GATING. (( J.A. Lasalde, S. Ortiz-Miranda, D. Butler, S. Tamamizu, C. R. T. Vibat, P. Pappone and M. McNamee.)) Section of Molecular and Cellular Biology, and Section of Neurobiology, Physiology and Behavior, Univ. of Calif., Davis, CA 95616.

Previous site-directed mutagenesis studies have shown that some conserved residues located at the putative lipid-protein interface of the *Torpedo californica* acetylcholine receptor may play a key role in the channel gating mechanism. The αC418W mutant, located in the M4 transmembrane domain, showed a 20-fold increase in channel open time when expressed in *Xenopus laevis* oocytes (Lee Y., et al., Biophys J. 66:646-653, 1994). Burst analysis of this mutant showed a 10-fold increase in the opening rate (β) when compared to the WT channel. It is remarkable that a single amino acid substitution in this region could have such dramatic effects. In order to build a model that can explain our results the following criteria have been used to construct a new series of mutants: conservation of the residue among various species, hydrophobicity, size, and relative position in the bilayer. Ten new mutants were constructed at the following WT positions of the α-M4 transmembrane domain: SER424, GLY421, CYS412 and two double mutants C418W-G421A and C418W-G421W. We used burst analysis to examine the kinetic behavior of these mutants. Our results show that some of these mutants produce: (1) an increased normalized macroscopic response to ACh, (2) an increased block induced by the agonist, and (3) a dramatic change in the gating properties of the channel. A detailed kinetic analysis will be presented. (Supported by USPHS Grants NS22941 and NS 13050.)

W-AM-B5

EXAMINATION OF THE NICOTINIC ACETYLCHOLINE BINDING SITE USING UNNATURAL AMINO ACID MUTAGENESIS. ((M. W. Nowak[1], P. C. Kearney[1], M. E. Saks[1], J. R. Sampson[1], W. Zhong[2], S. Silverman[2], C. Labarca[1], P. Deshpande[1], J. Thorson[3], E. Chapman[3], J. Abelson[1], N. Davidson[1], P.G. Schultz[3], D. A. Dougherty[2], and H.A. Lester[1])), [1]Div. of Biology, [2]Div. of Chemistry, Caltech, Pasadena, CA 91125, [3]Dept. of Chemistry, Univ. California, Berkeley, CA 94720. (Spon. by C. Brokaw).

We have adopted the stop codon suppression method for incorporation of unnatural amino acids into the mouse nicotinic acetylcholine receptor (nAChR) in a *Xenopus* oocyte expression system. *Xenopus* oocytes are coinjected with two RNAs: 1) cRNA synthesized from a mutated cDNA containing a TAG stop codon at the position of interest and 2) a suppressor tRNA containing the corresponding anticodon, CUA, chemically acylated with the unnatural amino acid. During protein synthesis, the aminoacylated suppressor tRNA directs the incorporation of the amino acid into the desired position of the protein.

As a test of the efficacy of the stop codon suppression method we incorporated the natural tyrosine (Y) residue at positions 93, 190 and 198 in the α subunit. Oocytes coinjected with αY93TAG, αY190TAG or αY198TAG cRNA along with the β, γ, and δ cRNAS and $tRNA_{CUA}$-Y yielded ACh-induced currents with a concentration-dependence and Hill coefficient indistinguishable from wildtype receptor. As a further test, oocytes coinjected with AChR αY198TAG and $tRNA_{CUA}$-phenylalanine (F) yielded electrophysiological properties identical to the AChR αY198F mutant examined using conventional mutagenesis.

To further examine the interaction of ligands with tyrosine residues in the α subunit we have introduced derivatives of tyrosine and phenylalanine at positions α93, α190 and α198. Subtle chemical changes in the tyrosine side chain produced measurable changes in the electrophysiological properties of nAChR.

Support: NIH, NRSA, NSF.

W-AM-B6

LEUCINE RESIDUES AT THE 9' POSITION OF THE M2 DOMAIN IN ACHR GOVERN EC50 INDEPENDENTLY AND SYMMETRICALLY. ((C. Labarca, M. W. Nowak, L. Tang, P. Deshpande, N. Davidson and H. Lester)) Divison of Biology, Caltech, Pasadena, CA 91125.

All known subunits of the acetylcholine receptor, both muscle and neuronal, have a leucine at approximately the midpoint of the M2 transmembrane domain (position 9'). Mutation of this leucine to several other residues, including serine, on the chick alpha7 neuronal receptor produces a large leftward shift in the dose-response for acetylcholine and drastically slows desensitization (Revah et al. 1991). Mutation of Leu9' to cysteine in the alpha subunit of the mouse receptor shifts the dose-response relation to the left by about one order of magnitude (Akabas et al. 1992). We have expressed in *Xenopus* oocytes mouse nAChR receptors with varying numbers of Leu9'Ser mutated subunits. The dose-response relation for ACh shifts to the left by a roughly constant factor, corresponding to a ten-fold decrease in the EC50, for each Leu9'Ser mutation. The additive effect of these mutations suggests that each Leu9' residue participates nearly independently in the transition between the closed and open states of the receptor. Hydrophobic interactions between Leu9' and other protein residues probably play an impoprtant role in AChR gating, perhaps restraining spontaneous opening of the channel. Large decreases in maximum current with increasing number of mutations also suggests a role for these residues in assembly of the receptor. Support: NIH, TRDRP.

**W-AM-B7**

AN ATP-ACTIVATED NON-SPECIFIC CATION CHANNEL IN GUINEA PIG VENTRICULAR MYOCYTES. ((K.E. Parker and A. Scarpa)) Case Western Reserve University School of Medicine, Department of Physiology and Biophysics, Cleveland, OH 44106

Extracellular ATP released from nerves onto vascular smooth muscle or released from damaged tissues during traumatic injury, shock or ischemia profoundly alters cardiovascular physiology. We used patch-clamp methods to investigate the effects of extracellular ATP on guinea pig ventricular myocytes because guinea pigs are a commonly used model for the study of cardiac electrophysiology. ATP activates a rapid, desensitizing, inward current. This inward current is activated by a $P_2$ receptor that does not conform to published receptor sub-classes. 100 uM ATP activates more current than 100 uM alpha-beta-methylene ATP, which activates more current than 100 uM ADP. 2-methylthio ATP and ATP-gamma-S are also effective agonists. Adenosine, AMP, GTP and UTP are ineffective at 100 uM. The inward conductance has a reversal potential near 0 mV and in ion-substitution experiments was found to be carried through non-specific cation channels rather than chloride channels. The conductance has inwardly rectifying current-voltage relations. When ATP is used as the agonist, fluctuation analysis yields an apparent unitary conductance of 0.08 pA at a holding potential of -120 mV with sodium as the main charge-carrying ion. Preliminary experiments using fluctuation analysis to determine dominant time constants with different agonists will be presented.

**W-AM-B8**

DEFINING THE LINK BETWEEN LIGAND BINDING AND GATING OF A CHLORIDE CHANNEL GATED BY GLUTAMATE. (A. Etter, B. Reiss, K. Liu, D. Cully, J. Schaeffer & J. Arena) Merck Research Labs, Rahway, NJ 07065 (Spon. by J. Arena)

We recently reported the cloning of two subunits (GluClα and GluClβ) of a glutamate-gated chloride channel from the free living nematode *Caenorhabditis elegans* (1). Homomeric GluClα and GluClβ channels expressed in *Xenopus* oocytes show different biochemical, pharmacological and electrophysiological properties. GluClβ is sensitive to glutamate ($EC_{50}$ of 400 μM). In GluClα, a glutamate-sensitive current can only be observed if channels are preactivated with ivermectin ($EC_{50}$ = 7 μM). This result suggests that glutamate either binds to a site on GluClα and the coupling to gating is impaired, or that glutamate binding occurs only in the presence of ivermectin. We have created a hybrid molecule with the amino terminal domain of GluClα (the putative ligand binding domain) and the carboxyl terminal part of GluClβ (the presumed pore). The chimeraic molecule was sensitive to glutamate in the absence of ivermectin with an estimated $EC_{50}$ of 260nM suggesting that glutamate binds to GluClα but that the coupling to the gating process is inefficient. If this hypotheses is valid, it should be possible to restore the glutamate sensitive current by altering amino acids in regions involved in the gating process such as the second membrane spanning helix (M2). We have introduced a point mutation in this region by exchanging a threonine for an alanine. This construct responded to high concentrations of glutamate ($EC_{50}$ = 6mM) and the maximum current elicited by glutamate was about 10% of the maximal current evoked by ivermectin. This result is consistent with a low efficiency gating mechanism. Results suggest that glutamate can bind to GluClα and the ionophore is impaired in its gating mechanism. (1) Cully, D.F., *et al*, *Nature* in press.

**W-AM-B9**

EXPRESSION AND CHARACTERIZATION OF A CLONED HIGH AFFINITY SULFONYLUREA RECEPTOR. ((L. Aguilar-Bryan, J. Clement, D.A. Nelson and J. Bryan)) Depts of Cell Biology and Medicine, Baylor College of Medicine, Houston, TX 77030

A radioiodinated derivative of the antidiabetic agent glyburide was used to photolabel and purify the pancreatic high affinity sulfonylurea receptor. N-terminal sequence was used to generate PCR primers and screening probes. cDNAs for the hamster and rat receptors have been sequenced and encode membrane glycoproteins of 177,209 and 177,102 daltons respectively. The two receptors are ~ 98% identical and are novel members of the ATP-binding cassette superfamily with two putative nucleotide binding folds (NBFs). Hydrophobicity analyses suggest a model with 13 transmembrane spanning domains: 9 domains before the first NBF and four domains between the two NBFs. Transient expression in COSm6 cells, which have no detectable endogenous receptor, gives 140 pmol of the hamster receptor/mg membrane protein; $K_D$ ~ 10 nM and 28 pmol/mg; $K_D$ ~ 2 nM for the rat. The hamster level is ~ 100-fold greater than that found in hamster insulinoma tumor (HIT) cells. Expression of the N-terminal half of the receptor gives no binding activity. $^{86}$Rubidium efflux studies on COSm6 cells overexpressing the receptor give no indication of novel $K^+$ currents following metabolic block with 2-deoxyglucose and oligomycin, a treatment that strongly activates $K_{ATP}$ in rat insulinoma (RIN) cell controls. The results are consistent with a model for the $K_{ATP}$ channel where the sulfonylurea receptor modulates a potassium selective pore. Work is in progress to couple the receptor to cloned, sulfonylurea insensitive members of the small inward rectifier family.

## STIMULUS-SECRETION COUPLING

**W-AM-C1**

EXCITATION-SECRETION COUPLING IN CULTURED RAT CHROMAFFIN CELLS IS GATED PRIMARILY BY THE L-TYPE $Ca^{2+}$ CHANNEL. ((L. Cleemann, J. Fan, B. Lara, L. Gandia, and M. Morad)) Department of Pharmacology, Georgetown University, Washington, DC 20007. (Spon. by G. Maréchal)

Rat adrenal chromaffin cells were enzymatically dispersed, strained through a nylon mesh, purified on a sucrose gradient, and maintained in culture up to one week. Single chromaffin cells (diameter: 15-30 μm; capacitance: 10-20 pF) were whole cell clamped and unitary secretory events were simultaneously monitored as oxidation current (max. 50 pA • 20 ms) using carbon fiber electrodes (diameter 6-8μm). In control Tyrode's solutions the activation of a large $Na^+$ current (≈100 pA/pF) was accompanied by a smaller, slowly inactivating composite of $Ca^{2+}$ currents (≈5 pA/pF) and a small time-dependent outward current (possibly $Ca^{2+}$-activated). In $Cs^+$-dialyzed cells, the latter current required $[K^+]_o$ and was absent in cells buffered with 5mM EGTA. Secretory events were recorded consistently in cells dialyzed with 0.1mM BAPTA on activation of $I_{Ca}$. During depolarizing pulses to +10mV, secretory activity increased to a maximum within 200ms and fell rapidly on repolarization. The voltage dependence of secretion and $I_{Ca}$ were similar and bell-shaped. Partial block (20-40%) of the $Ca^{2+}$ current by 10μM nifedipine was accompanied by nearly complete cessation of secretion and suppression of the $Ca^{2+}$-dependent outward current. We conclude that although a small fraction (≈20%) of total $Ca^{2+}$ current is carried by the L-Type channels, this current is crucial in gating the secretory process. Supported by NIH HL16152 and NATO CRG 900986.

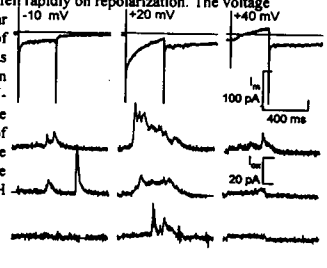


**W-AM-C2**

ANTIBODIES SPECIFIC TO DIVERGENT REGIONS WITHIN THE INTRACELLULAR DOMAIN (II-III LOOP) OF N-TYPE ALPHA1 SUBUNIT IDENTIFY SPECIFIC VARIANTS.
((M.W. McEnery, W.L. Lee, T.D. Copeland+, M. Pacioianu, and C.M. Begg))
Department of Physiology and Biophysics, Case Western Reserve University School of Medicine, Cleveland, OH 44106-4970,+ABL-Basic Res. Prog., NCI-Frederick Cancer R&D Center, Frederick, MD 21702,))

The molecular cloning of the N-type alpha1 subunits from several mammalian species (Dubel, et al. 1991; Williams, et al. 1991) facilitates the search for structural variants of the alpha1 subunit. The strategy outlined in this study utilizes epitope-specific anti-peptide antibodies raised to sequences found in 1) all VDCC alpha1 subunits, 2) all N-type specific VDCC, and 3) highly divergent domains that are unique to specific cDNA clones (rat or human). All antibodies were affinity purified and characterized by western blot analysis of a variety of neuronal and non-neuronal tissues and immunoprecipitation of [$^{125}$I]omega-conotoxin GVIA binding from solubilized samples. The results indicate that discrete epitopes present in cDNA clones can be used to generate variant-specific antibodies. Using these antibodies, we have examined the possibility that several N-type VDCC alpha1 subunit may be expressed in a single tissue. Also, as several of our antibodies immunoprecipitated [$^{125}$I]CTX binding quantitatively, we are investigating the co-immunoprecipitation of other proteins which may form persistent complexes with the N-type alpha1 subunit.

**W-AM-C3**

INTERACTIONS OF A POTENTIAL REGULATORY PROTEIN WITH THE GASTRIC $H^+/K^+$ ATPase. J. Cuppoletti, A. M. Rubtsov*, G. Behbehani, and O. D. Lopina*. Dept. Mol. and Cell. Physiol. and Int. Med., Univ. Cinc. Coll. Med., Cincinnati, OH 45267-0576 and *Visiting Professors from Dept. Biochem. Moscow State Univ., 119899, Moscow, Russia.

A 67 kDa cytosolic protein with melittin-like determinants which exhibits stimulus-associated interactions with gastric $H^+/K^+$ ATPase-containing membranes [(AJP GI&L 27):G637-G644,1993] was partially purified using anti-melittin antibody affinity columns. When mixed with $H^+/K^+$ ATPase-containing vesicles from non-secreting rabbit gastric mucosae, the extent of ATP driven HCl accumulation by the vesicles was greatly increased. A polypeptide binding site within the cytosolic domain of the gastric $H^+/K^+$ ATPase has recently been localized to residues $I_{603}$DPPRAT. This sequence, when included within a 45 amino acid synthetic polypeptide based on the sequence of the gastric $H^+/K^+$ ATPase which flanks this region, was phosphorylated by PKA. Binding of melittin and the 67 kDa protein to this peptide in the phosphorylated and unphosphorylated form was evaluated with a fluorescently labeled analog of the synthetic polypeptide modified at a single cysteine residue by with ammonium 4-chloro-7-sulfobenzofurazan (SBF-Cl). Melittin decreased the fluorescence of the unphosphorylated form in a dose-dependent manner, with high affinity and a stoichiometry of 1:1. A similar decrease in fluorescence was observed with the 67 kDa protein. Phosphorylation of the synthetic peptide prevented interaction. These functional and structural studies suggest direct interactions of the 67 kDa protein with the gastric $H^+/K^+$ ATPase. Supported by DK43816 and DK43377 to JC.

**W-AM-C4**

STIMULUS INDUCED CHANGES IN CYTOPLASMIC FREE SODIUM IN SECRETORY NERVE ENDINGS. ((D. Turner and E.L. Stuenkel)) Department of Physiology, Univ. of Michigan, Ann Arbor, MI 48109

The level and extent of exocytosis is regulated by the electrical activity of neurons via induced changes in the free intracellular calcium concentration. However, a role for $Na^+$ in enhancement of neurotransmitter release has also been suggested from $Na^+$ loading of nerve endings by tetanic stimulation, direct $Na^+$ injection and pharmacological blockade of the $Na^+$-pump. We have previously demonstrated that in peptide secreting nerve endings of the neurohypophysis $Na^+$ can have a direct, $Ca^{2+}$-independent effect to enhance secretion. In the present study we have used fluorometric monitoring of $[Na^+]_i$ simultaneous with whole cell voltage clamp of single isolated nerve endings to determine the amplitude and kinetics of stimulus induced changes in $[Na^+]_i$ in response to stimuli of duration and frequency similar to that of action potentials in vasopressinergic nerve endings. Application of brief repetitive depolarizing commands (-90 mV holding potential, +10 or -10 mV step potentials of 2 msec duration) results in increases in the $[Na^+]_i$. The stimulus evoked increases in $[Na^+]_i$ occurred at frequencies as low as 5 Hz. Both the amplitude and rate of increase in $[Na^+]_i$ were directly dependent upon the stimulation frequency. Stimulus evoked increases in $[Na^+]_i$ were blocked by application of 0.3 $\mu$M tetrodotoxin, as were the inward $Na^+$ currents. Additional experiments in which the recording pipette contained 9 mM $Na^+$, to approximate a normal cytoplasmic $[Na^+]_i$, have also demonstrated stimulus induced increases in $[Na^+]_i$ beginning at frequencies of 10 Hz. The findings suggest that action potentials in neurohypophysial nerve endings are capable of raising $[Na^+]_i$ to levels which can directly modulate basal and $Ca^{2+}$-dependent peptide secretion.

**W-AM-C5**

GLUCOSE AND SULFONYLUREAS BLOCK THE Na/K PUMP IN A PANCREATIC $\beta$ CELL LINE. ((B. Ribalet)) Dept. of Physiology, UCLA, Los Angeles, CA 90024.

The Na/K pump current was recorded in insulin secreting cells using the whole-cell patch clamp configuration, with the pipette solution containing in mM: 100 NMDG, 40 NaCl, 10 Hepes, 10 EGTA, 1 $CaCl_2$, 4 ATP and 4 $MgSO_4$. With a bath solution of 140 TEA, 10 Hepes and 1.2 $MgSo_4$ addition of 2 mM KCl to the bath induced an outward current which was almost completely blocked by 1$\mu$ M ouabain. This current, which is attributed to the activation of the Na/K ATPase, was dependent upon the intracellular concentration of ATP. Below 1 mM ATP the current was negligible. At 5 to 7 mM ATP the current reached a maximum of 2.5 to 5 pA. The Na/K pump current was blocked by glucose at concentrations greater than 5 mM and by the sulfonylurea glyburide (10 nM). These results are consistent with the hypothesis that in pancreatic $\beta$ cells the sulfonylurea receptor interacts not only with the ATP-dependent K channel, but also with the Na/K pump. Thus the blockage of the Na/K pump by glyburide and its dose-dependent inhibition by glucose may be responsible for the modulation of insulin release observed at glucose concentrations greater than 5 mM. However, even within this scheme, inhibition of the $K_{ATP}$ channel by less than 5 mM glucose or glyburide is required to depolarize the membrane and initiate insulin release.

**W-AM-C6**

GLUCOSE TRANSIENTLY ACTIVATES CYTOSOLIC $Ca^{2+}$ RELEASE IN MOUSE ISLETS BY A PHOSPHOLIPASE C-DEPENDENT MECHANISM ((M.W. Roe, G. Campbell, B. Spencer, M.E. Lancaster, J.F. Worley III and I.D. Dukes)) Glaxo Research Institute, RTP, NC 27709; University of Chicago, Chicago, IL 60637.

Increasing glucose concentration from 2 to 12mM elicits a triphasic alteration of C57BL/KsJ mouse pancreatic islet cytosolic $Ca^{2+}$ concentration ($[Ca^{2+}]_i$), with an initial thapsigargin-sensitive reduction (phase 0) followed by a transient caffeine-sensitive elevation (phase 1) stemming from intracellular $Ca^{2+}$ release, and $[Ca^{2+}]_i$ oscillations (phase 2) dependent on $Ca^{2+}$ influx through L-type voltage-dependent $Ca^{2+}$ channels. Consistent with these results, we found that exposure of islets to 500nM nitrendipine totally inhibited glucose-stimulated phase 2 $[Ca^{2+}]_i$ oscillations while phase 1 was only partially diminished. Administration of carbachol or the phospholipase-C inhibitor U-73122 prior to glucose stimulation ablated phase 1, and reduced the amplitude and increased the frequency of phase 2 $[Ca^{2+}]_i$ oscillations. Incubation in the presence of 0.5mM diazoxide (DZ) for the first minute of a 12mM glucose exposure suppressed the development of phase 1 following DZ washout, and suggested that the intracellular signal activating cytosolic $Ca^{2+}$ release was present only for a brief period after glucose stimulation. After removing DZ following longer incubations (>5 min), 12mM glucose induced a series of large caffeine-sensitive $[Ca^{2+}]_i$ transients. Our findings confirm that glucose stimulates transient intracellular $Ca^{2+}$ mobilization, and suggest that a caffeine sensitive intracellular $Ca^{2+}$ store might also regulate phase 2 $[Ca^{2+}]_i$ oscillations. We conclude that the phase 1 $[Ca^{2+}]_i$ transient is due to the release of intracellular $Ca^{2+}$ via a phospholipase C-dependent mechanism activated by membrane depolarization.

**W-AM-C7**

CYTOSOLIC GRADIENTS DURING GLUCOSE-INDUCED $[Ca^{2+}]_i$ OSCILLATIONS IN MOUSE PANCREATIC ß-CELLS. ((B. Soria, J. Ribas # and F. Martin)) Dept of Physiology, University of Alicante and (#) Dept. of Physiology and Biophysics, University of Sevilla, Spain.

It has been previoulsy found in mouse pancreatic islets that glucose induces oscillations of cytosolic $Ca^{2+}$ which are due to bursting of electrical activity (Pflügers Arch. 1991:418, 417-422). Average $[Ca^{2+}]_i$ oscillations are square shaped and their duration correlates with glucose-induced insulin release. It has been suggested that is the duration of these oscillations what encodes for sustained insulin release. The aim of the present work is to find out whether during steady-state 11 mM glucose-induced oscillations $Ca^{2+}$ is uniformely distributed whithin the ß-cell. Methods: islets were obtained by collagenase digestion and used in 4-8 h. ß-cells were dissociated, plated and used during the first 4-8 h. $[Ca^{2+}]_i$ was monitored using indo-1. The imaging system consists on a inverted fluorescence microscope, a CCD camera and a host microcomputer. Samples were taken each 5 s. A deblurring algorithm previously described was used (J. Cell Biol 116:745-759).
Results: 1. Ca2+ gradients in isolated ß-cells. In dissociated ß-cells from mice islets a clear gradient in the glucose-induced response was observed. No clear $[Ca^{2+}]_i$ oscillations were observed in dissociated cells. 2. Gradients in ß-cells whitin the islet. Contrariwise to dissociated cells, mice pancreatic islets develop robust oscillations of $[Ca^{2+}]_i$ when challenged with 11 mM glucose. Fluroresecence digital image analysis one single cell which oscillates with the same period showed that $[Ca^{2+}]_i$ distribution whithin the ß-cell is not homogeneous. Fluorescence appears at one pole and reaches values which are 2-3 fold those observed in the other pole.

**W-AM-C8**

SLOW $[Ca^{2+}]_i$ OSCILLATIONS INDUCED BY AMINO ACIDS IN MOUSE PANCREATIC ISLETS OF LANGERHANS. ((F. Martin and B. Soria)) Dept. of Physiology and Institute of Neurosciences, University of Alicante School of Medicine, Alicante, Spain. (Spon. by C. Ripoll).

The effects of exogenous amino acids on $[Ca^{2+}]_i$ oscillations in islets perifused with 5 mM or 11 mM glucose were studied. Plasma amino acid concentrations were determined in fed or 24 h fasted animals. Islets were superfused in vitro with solutions mimicking plasma composition in fed (total amino acid 2.55 mM, D-glucose 11 mM) or fasted (total amino acids: 2.77 mM, D-glucose 5 mM). 1. Slow $[Ca^{2+}]_i$ oscillations appeared when islets were incubated with a solution containing a mixture of amino acids and glucose which reproduce the situation of a fed animal. 2. While, in the presence of 11 mM glucose, alanine (5 mM) and arginine (5 mM) induced a transient rise of $[Ca^{2+}]_i$, leucine (3 mM) and isoleucine (10 mM) triggered slow $[Ca^{2+}]_i$ oscillations. 3. In the presence of glucose (11 mM), tolbutamide (10 $\mu$M) increased the duration and the amplitude of $[Ca^{2+}]_i$ oscillations. While tolbutamide (10 $\mu$M) slightly broadened the leucine-induced slow oscillatory pattern, addition of diazoxide (10 $\mu$M) resulted in the gradual appearance of $[Ca^{2+}]_i$ oscillations which ressemble glucose-induced fast oscillations. 4. Fluoroacetate (2 mM) transformed leucine-induced slow $[Ca^{2+}]_i$ oscillations into fast ones. Iodoacetate (1 mM) completely inhibited any oscillatory pattern. 5. It is suggested that mitochondrially generated signals derived from amino acid oxidative metabolism acting in conjunction with glucose-signaled messengers are very effective at closing ATP-dependent $K^+$ channels ($K^+_{ATP}$).

**W-AM-D1**

**EFFECT OF DMSO AND MICELLES ON HEMIN AGGREGATION AS MONITORED BY OPTICAL ABSORPTION SPECTRA AND CATALYSIS OF CHEMICAL REACTIONS.** ((S.E.K. Sampaio, E. Linares, M.C.A. Ribeiro, A.M.C. Ferreira and S. Schreier)) Instituto de Química, Universidade de São Paulo, C.P. 20780, 01498-970, São Paulo, SP, Brazil. (Spon. by M.T. Lamy-Freund)

Hemin (Fe3+-protoporphyrin IX) is a lytic agent and a catalyst of oxidative reactions. We have shown that the mechanism of lysis depends on hemin's aggregation state (Schmitt et al, *Arch. Biochem. Biophys.* **307** (1993) 96): while monomers catalyse lipid peroxidation, higher aggregates intercalate in the membrane, changing the molecular packing. Here, we examined the effect of micelles and dimethyl sulfoxide (DMSO) on hemin's aggregation state, both by optical spectroscopy and by following the kinetics of hemin-catalysed reactions: $H_2O_2$ decomposition, as well as formation and further reduction of 2,2'-azinodi(3-ethylbenzthiazoline)-6-sulfonate (ABTS) cation radical. The ABTS reactions were monitored both by absorption spectra and by EPR. The reaction rates increased in the presence of DMSO and/or detergents. This effect was paralleled by an increase in monomeric hemin. Thus, both agents are capable of shifting the monomer-dimer equilibrium. The results also indicate that both species are present in the presence of micelles.

Financial support: FAPESP, CAPES,CNPq.

**W-AM-D2**

**EFFECTS OF LIPID MEMBRANE ENVIRONMENT ON THE STRUCTURE AND AGGREGATION PROPERTIES OF NICKEL PORPHYRINS**

((X. Song,[1,2] M. Miura,[3] J. D. Hobbs,[1] J. Cesarano[1] and J. A. Shelnutt[1,2])) [1] Fuel Science and Ceramic Processing Science Departments, Sandia National Laboratories, Albuquerque, NM 87185-0710. [2] Department of Chemistry, University of New Mexico, Albuquerque, NM 87131. [3]Department of Applied Science, Brookhaven National Laboratory, Upton, NY 11973.

Metalloporphyrins, because of their photochemical activity and capacity of modification by peripheral substitution, could be widely used in molecular sensors, electronic and photo-active devices. Langmuir-Blodgett (LB) film technology can be used to organize the active components in an ordered fashion. A lipo-porphyrin, Ni(II) 2,3,7,8,12,13,17,18-octaaceticacid-5,10,15,20-tetra(phenyl-eicosanate)-porphyrin (NiLipoP), has been computer-designed as a protein recognition site for cytochrome *c* at the surface of lipid LB film and its octamethyl ester (NiLipoP-OME) has been synthesized. NiLipoP-OME and, for comparison, Ni protoporphyrin IX dimethyl ester (NiPPDME), have been incorporated into stearic acid LB films. Effects of the lipid membrane environment on the structure and aggregation properties of these porphyrins have been investigated by UV-visible absorption spectroscopy and resonance Raman spectroscopy. Molecular mechanics calculations were carried out to aid the interpretation of the spectral and physical properties. Our results show that NiPPDME exists in an equilibrium between planar and nonplanar forms in $CH_2Cl_2$ solution. After incorporated into lipid LB film, NiPPDME is mostly planar probably as a result of aggregation. In contrast, the highly nonplanar NiLipoP shows no evidence of aggregation or structural change after incorporated into the film. Molecular modeling suggest that the polar porphyrin head group lies above the surface of the stearic acid film, making the molecular recognition site accessible to the solvent for protein-binding. (Supported by United States Department of Energy Contract DE-AC04-94AL85000 and Associated Western Universities Fellowships (XS JDH).)

**W-AM-D3**

**NON-PLANAR FLUORINATED METALLOPORPHYRINS: EFFECTS OF ELECTRON WITHDRAWING PERIPHERAL SUBSTITUENTS.** ((M.C. Simpson[1], K.K. Taylor[1,4], J.D. Hobbs[1], C.J. Medforth[2], T.P. Forsyth[2], K.M. Smith[2], K.M. Kadish[3], and J.A. Shelnutt[1,4])) [1]Fuel Science Department, Sandia National Laboratories, Albuquerque, NM 87185-0710. [2]Department of Chemistry, University of California, Davis, CA 95616. [3]Department of Chemistry, University of Houston, Houston, TX 77204-5641. [4]Department of Chemistry, University of New Mexico, Albuquerque, NM 87131.

**Metalloporphyrins (MPs) hold promise as base molecules from which to rationally design biomimetic catalysts. To effectively tailor MPs for desired reactions, the steric and electronic effects of structural modifications upon the macrocycle must be determined. To elucidate the origins of established structure-spectrum correlations, we separated steric and electronic contributions to observed behavior by synthesizing and characterizing two series of porphyrins: 1) variably fluorinated phenyl-substituted $Fe^{III}$ and $Ni^{II}$ porphyrins, for which the electronic nature of the peripheral substituents varies without significant steric changes, and 2) meso-substituted tetraalkyl porphyrins that have variable nonplanar distortions with almost constant electronic substituent properties (see poster by W. Jentzen, this meeting). We report resonance Raman studies on the first of these two series: $F_x$DPPFeCl (x=0,20,28,36); $F_x$DPPNi (x=0,20,28,36); $F_x$TPPFeCl (x=0,8,20); $F_x$TPPNi (x=0,8,20); $F_x$OETPPFeCl (x=0,20). The negligible steric effect of the fluorines is confirmed by molecular mechanics calculations using a new, optimized classical forcefield. Shifts of structural marker lines can be attributed to the electronic character of the peripheral substituents. This argument is supported by linear correlations among the Raman marker lines, the net electron withdrawing capacity of the substituents, and the porphyrin redox properties.** (Supported by U.S. Dept. of Energy Contract DE-AC04-94AL85000, Associated Western Univ. (KKT, JDH, CJM) and a D.O.E. Distinguished Postdoctoral Fellowship (MCS).)

**W-AM-D4**

**RUFFLING IN A SERIES OF NICKEL TETRAALKYLPORPHYRINS AS A MODEL FOR THE CONSERVED RUFFLING OF THE HEME OF CYTOCHROME *C*.**

((W. Jentzen,[1] J.D. Hobbs,[1] X.Song,[1,2] M.C. Simpson,[1] K.K. Taylor,[1] T. Ema,[3] N.Y. Nelson,[3] C.J. Medforth,[3] K.M. Smith,[3] M. Veyrat,[4] M. Mazzanti,[4] R. Ramasseul,[4] J.-C. Marchon,[4] T. Takeuchi,[5] W.A. Goddard III,[5] J.A. Shelnutt,[1,2])) *[1]Sandia National Laboratories, Albuquerque, NM 87185-0710, [2]University of New Mexico, Albuquerque, NM 87131, [3]University of California, Davis, CA 95616, [4]CEA/Laboratoire de Chimie de Coordination, 38054 Grenoble, France, [5]California Institute of Technology, Pasadena, CA 91125.*

**Metalloporphyrins undergo remarkable nonplanar distortions of the macrocycle that perturb the chemical and photochemical properties of these protein cofactors. Further, the tertiary structure of the surrounding protein can manipulate these distortions as a means of regulating biological function. In cytochromes *c*, for example, a highly conserved nonplanar distortion of the heme exists and likely plays a role in electron-transfer since the distortion is maintained by the protein at significant energetic expense. This heme distortion is primarily of the ruffling (*ruf*) type in which the pyrroles are twisted about the metal-$N_{pyrrole}$ bond. Substitution of the porphine molecule with tetrahedrally bonded atoms at the four *meso* bridging carbons generally results in the *ruf* distortion; therefore, we investigated a series of tetra*alkyl*porphyrins in which the alkyl substituents vary in size (methyl, ethyl, pentyl, isopropyl, cyclopropyl-1a, cyclohexyl, myrtenyl, *t*-butyl, adamantyl). Molecular mechanics calculations show that increasing steric crowding at the periphery results in higher degrees of ruffling in the series ($C_aNNC_a$ angle, 0 to 57°), and generally agree with the X-ray structures available. Raman structure-sensitive lines decrease nonlinearly with increasing ruffling angle as bond force constants change with torsion angles. Absorption bands red shift nonlinearly as predicted by MO calculations.** (Supported by U.S. DOE Contract DE-AC04-94AL85000 and Associated Western Universities Fellowships (WJ, XS, JDH, KKT), and a DOE Distinguished Postdoctoral Fellowship (MCS))

**W-AM-D5**

**LIGAND BINDING KINETICS AND ELECTRONIC STRUCTURE OF FE(II)-$O_2$ AND FE(II)-CO BONDS IN HEMOPROTEINS AND HEME MODELS.**

((D. Lavalette, D. El-Kasmi, M. Momenteau and C. Tetreau))
INSERM U350 & CNRS URA1687, Institut Curie, 91405-Orsay France.

The overall reactivity of hemoproteins roots primarily in the electronic factors affecting the heme, whereas the globin provides substrate specificity and additional modulation.Recent kinetic investigations of heme models in this laboratory have confirmed that the contrasted reactivity of oxygen-carrying hemoproteins and cytochromes P-450 towards oxygen and carbon monoxide is a consequence of the replacement of the proximal ligand of the heme (i.e. nitrogenous base *vs* thiolate). To get a deeper insight into the underlying electronic factors, we have determined the "on / off" rate parameters of $O_2$ and CO binding with a number of heme models using a series of proximal ligands spanning a range of $pK_a$ values from about 4 to 16. Upon increasing the $pK_a$ of the proximal ligand, the dissociation rate of CO complexes increases, whereas all other rate parameters are found to decrease. These findings account for the opposite variation of the equilibrium constants and for the strong stabilization of $O_2$ complexes compared to CO complexes by highly basic proximal ligands. Our data provide an experimental support to quantum chemical calculations predicting a preferential stabilization of the Fe(II)-$O_2$ bond by $\pi$ back-bonding.

**W-AM-D6**

**CHEMICAL MODELING OF CYTOCHROMES P-450: KINETICS OF $O_2$ AND CO BINDING.**

((C Tetreau, D. El-Kasmi , M. Momenteau and D. Lavalette ))
INSERM U350 & CNRS URA1687, INSTITUT CURIE, 91405-Orsay France.

The combination of chemical modeling and of laser flash photolysis studies has markedly contributed to the understanding of environmental factors governing the reactivity of the active site of oxygen-carriers. Over the past 20 years, numerous heme models of cytochromes P-450 have been designed by replacing the nitrogenous proximal ligand found in oxygen carriers by a thiolate residue. However their reactivity has remained almost unexplored: only three kinetic investigations of CO binding were previously reported and kinetic data for $O_2$ binding are missing. In the present work, we have investigated the kinetics of $O_2$ and CO binding with thiolate five-coordinated complexes of several porphyrin structures using laser flash photolysis. We report full kinetic data for 5 carbonylated and 4 oxygenated species. Our models reproduce the large decrease of M= $K_{CO}/K_{O2}$ exhibited by cytochromes P-450 compared to $O_2$-carriers and exhibit linear free energy relationships (LFER) close to those of cytochrome $P\text{-}450_{scc}$. Kinetic dissociation rates indicate that the stability of the CO and $O_2$ complexes are respectively decreased and increased upon replacing the nitrogenous proximal ligand by a thiolate. These opposite trends account for the decrease of $K_{CO}$ and the concomitant increase of $K_{O2}$ responsible for the changes in M from $O_2$-carriers to cytochromes P-450.

W-AM-D7

MICROSECOND KINETICS OF THE REACTION OF OXYGEN WITH CYTOCHROME *c* OXIDASE STUDIED BY RAPID SOLUTION MIXING ((Satoshi Takahashi, Yuan-chin Ching, Jianling Wang and Denis L. Rousseau)) AT&T Bell Laboratories, Murray Hill, NJ 07974

Cytochrome *c* oxidase binds molecular oxygen at its cytochrome $a_3$ site to make the first of a series of intermediates that result in the oxygen being reduced into water. The investigation on this process by directly mixing the enzyme with oxygen has been impossible, because with a conventional stopped flow apparatus the mixing dead time (~ms) is longer than the enzyme's turnover. Information on the intermediates so far has therefore been obtained by using CO-inhibited enzyme, from which CO can be photolysed to initiate the reaction. However, the photolysed CO might interfere with the reaction in a number of ways. To address this question, we have developed a rapid mixing device that can mix two solutions within several tens of μs, and the structure and kinetics of the oxygen bound enzyme has been detected by resonance Raman spectroscopy. The preliminary results show that the Fe-$O_2$ stretching frequency as well as the formation and decay kinetics of the primary intermediate are the same as those obtained by the CO-flash method. The implications of these results will be discussed.

W-AM-D8

STRUCTURAL DETERMINANTS OF COOPERATIVE OXYGEN BINDING IN *SCAPHARCA* HEMOGLOBINS ((William E. Royer, Jr. and Animesh Pardanani)) Program in Molecular Medicine and Dept. of Biochemistry & Molecular Biology, University of Massachusetts Medical Center, Worcester, MA 01605

The blood clam *Scapharca inaequivalvis* has intracellular dimeric and tetrameric hemoglobins, both of which exhibit cooperative oxygen binding. The assembly of their subunits is very different from that of mammalian hemoglobin which necessitates a very different cooperative mechanism. High-resolution crystal structures of liganded and unliganded *Scapharca* dimeric hemoglobin establish that cooperativity relies not on large subunit movements but rather on tertiary structural transitions involving the heme groups and a small number of residues. Additionally, ordered water molecules play important roles in stabilizing the alternate states of the interface. We have begun probing the roles of individual residues in the cooperative mechanism by site-directed mutagenesis. The structure of CO-liganded *Scapharca* tetrameric hemoglobin is being determined at 2.1Å resolution. Within the tetramer are two heterodimers that assemble similarly to the *Scapharca* homodimer suggesting that the basic cooperative mechanism is similar in both hemoglobins. Nonetheless, the greater cooperativity in the tetramer implies significant communication between the dimers whose oxygen binding sites are more than 45Å apart. (Supported by NIH and AHA)

W-AM-D9

WATCHING A PROTEIN AT WORK: THE CRYSTAL STRUCTURE OF PHOTOLYZED CARBONMONOXY MYOGLOBIN. ((Joel Berendzen, Ilme Schlichting, George N. Phillips, Jr.)) Biophysics Group, M715, Los Alamos National Laboratory, Los Alamos, NM 87545, Max Planck Institute for Medical Studies, Heidelberg, Germany, Department of Biochemistry, Rice University.

The oxygen storage protein myoglobin is the model system *par excellence* for physical studies aimed at understanding the relationship between protein structure and function. Single photons can break the covalent bond between the heme iron in myoglobin and carbon monoxide ligands; the ensuing rebinding process has been extensively studied as a model for the interplay of dynamics, structure, and function in protein reactions.

In what may be science's coolest movie, we have produced a sequence showing the intrepid protein before, during, and after its reaction with CO. We combined very low temperatures (to slow things down) with x-ray diffraction at a synchrotron source to obtain pictures of the CO-protein pair at atomic (1.5 Å) resolution. These pictures reveal that upon photolysis the CO lies flat atop the heme, some 4 Å from the iron, which itself has moved out of the plane of the heme 80% of the way towards its deoxy position. Other parts of the protein also assume high-energy conformations when the CO gets zapped off.

W-AM-D10

HOMOLOGY MODELING OF HORSERADISH PEROXIDASE AIDED BY 2D NMR ASSIGNMENTS. (G. H. Loew, P. Du and A. T. Smith) Molecular Research Institute, 845 Page Mill Road, Palo Alto, CA 94304.

Three dimensional (3D) models of horseradish peroxidase (HRP) and their Cyano complexes were constructed using the known structures of three other members of the plant peroxidase superfamily: cytochrome c peroxidase (CCP), lignin peroxidase (LiP), and *Arthromyces ramosus* peroxidase (ARP). Six models of the cyano complexes of the full protein, differing mainly in the conformation of a large insertion between helices F and G were obtained. Comparisons of the calculated distances between specific heme moieties and nearby residues in these models with those derived from 2D NMR data allowed the selection of one of these models as the most plausible and the identification of the Ile 180 as Ile-X residue responsible for a cross peak with the heme 8-CH3 group and Leu 250 as the aliphatic residue responsible for cross peaks with the proximal histidine 170 Cβ-protons deduced from NMR studies.

## MYOSIN

W-AM-E1

CALCIUM REGULATION OF MYOSIN I ISOLATED FROM URINARY BLADDER SMOOTH MUSCLE. (( Janek Sosinski and Samuel Chacko)) Department of Pathobiology, University of Pennsylvania, Philadelphia, PA 19104.

Pig urinary bladder smooth muscle contains a single headed monomeric myosin (myosin I) which has a 110 kDa heavy chain and 3-4 moles of 17 kDa light chains that are identical to calmodulin. Exogenous calmodulin is incorporated into isolated myosin I, until a maximum of 4 moles calmodulin per mole heavy chain is reached. When the heavy chain is saturated with calmodulin, the actin-activated MgATPase of myosin I is $Ca^{2+}$-sensitive. The kinetic mechanism of actin-activation of myosin I ATPase was investigated using smooth muscle actin. Double-reciprocal plot of ATPase activity *versus* actin concentration showed that the $V_{max}$ of actin-activation is unaffected by $Ca^{2+}$. However, $Ca^{2+}$ causes a three-fold increase in the $K_{ATPase}$ (the apparent binding constant of myosin I.ATP for actin). The actin-activated ATPase activity is inhibited two- and four-fold by smooth muscle tropomyosin and caldesmon respectively, but the inhibition is independent of $Ca^{2+}$. Hence, the actin-activated ATPase of myosin I from smooth muscle is regulated by $Ca^{2+}$, and this regulation is not dependent on the presence of tropomyosin or caldesmon. Supported by DK 39740 & DK 47514.

W-AM-E2

QUANTITATIVE ALIGNMENT OF THE MOLECULAR STRUCTURES OF MYOSIN-S1 AND ACTIN WITHIN THE ACTO-S1 RIGOR COMPLEX. ((R. A. Mendelson[1], E. P. Morris[2] and Z. Huang[3])) [1]C.V.R.I. & Biochem./Biophys., [3]Pharm. Chem., Univ. Calif. San Francisco, CA 94143; [2]Dept. Biochem., Imperial College London SW7 2BZ.

In order to define better the detailed structure of the rigor acto-S1 complex and the interacting groups at the interface between these proteins, we have conducted a quantitative search of their alignments. For this purpose we use the crystal structure of S1 (Rayment *et al., Science* 261: 50, 1993a) and the crystal structure of G-actin (Kabsch *et al., Nature* 347: 37,1990) in the filament alignment previously deduced (Holmes *et al., Nature* 347:44,1990; Mendelson and Morris, *J.M.B.* 240: 138, 1994) together with cryo-electron microscope data of the acto-S1 rigor complex (Milligan *et al., Nature* 348:217,1990; Rayment *et al., Science* 261:58,1993). Our approach is based on that previously described for F-actin: a systematic least-squares search of rotational and translational alignments fitted against the amplitudes and phases of non-equatorial layer-line data. The best alignment derived by these methods is close to the visual alignment of Rayment *et al* (1993b), but significantly different. Going from the visual alignment to our refined alignment yields an improvement in R-factor of 28%. In the improved alignment the two α-helices at the base of the 50kD segment straddle actin residues 342-357. These interactions appear to involve hydrophobic interactions between α-helices. Residues 405-425 in a loop in the upper 50kD segment of S1 now appear to interact with actin near residues 25-27. We are currently examining in detail the likely atomic interactions. (Supported by NIH AR39710 & AR42895)

**W-AM-E3**

THE CONFORMATION OF RHODAMINE DIMER IN THE SULFYHYDRYL ONE BINDING SITE OF MYOSIN. ((Katalin Ajtai and Thomas P. Burghardt)) Department of Biochemistry and Molecular Biology, Mayo Foundation, Rochester, MN 55905.

The dye 5' iodoacetamidotetramethylrhodamine (5'IATR) binds covalently as a dimer to the myosin subfragment 1 (S1). The nature of the dye-protein interaction was investigated using absorption, fluorescence polarization, and circular dichroism (CD) spectroscopy on several rhodamine dyes in solution (5'IATR, rhodamine 590, and rhodamine B). These data were combined with 2D-NMR data from the same systems to determine the conformations of the dimers. Dimer spectroscopic data were interpreted using a model based on coupled oscillating dipoles. The conformation of all the dimers have stacked xanthene rings in two distinct structures having very different spectroscopic signatures. The two structures of the 5'IATR dimer are equally likely in solution. Calculation of the CD signal from the 5'IATR indicates that the two conformations have signals of opposite sign on the absorption band of each dimer. Following the induced CD signal from 5'IATR binding to S1 shows that initially both conformations covalently link to S1. In time, the -CD signal disappears leaving only the +CD signal. The -CD dimer is converted to the +CD dimer (+dimer) by its interaction with S1. The dipoles of the +dimer are coupled to the dipoles of a tryptophan in the binding pocket of S1 to account for the spectroscopic properties of 5'IATR-S1. A correspondence is made between the spectroscopic fingerprint of 5'IATR-S1 and its interactions with the atoms local to the probe binding site. Supported by NIH (R01 AR 39288), AHA (930 06610), and the Mayo Foundation.

**W-AM-E4**

**MYOSIN S1-INDUCED MOTION OF SUBDOMAIN 2 IN F-ACTIN.** ((Andrzej A. Kasprzak)) *CRBM-CNRS, INSERM-U.249, Univ. Montpellier I, Montpellier, France*

In an effort to identify structural changes in the F-actin filament resulting from its interaction with myosin subfragment 1, distance measurements between Lys-61 on actin and 3 loci in the filament were performed in the absence and in the presence of S1. The technique to measure the distances was fluorescence resonance energy transfer (FRET). Fluorescently labeled actin was copolymerized with unlabeled actin in the presence of phalloidin. Since the fraction of the donor or doubly labeled protein in the filament was very low (0.03 - 0.05), the difficulties of taking into account multi-acceptor FRET were eliminated. Formation of the acto-S1 rigor complex resulted in a 30% decrease in FRET corresponding to the augmentation of the intramonomer actin distance from Cys-374 to Lys-61 by 6-7 Å. The change in the intermonomer distance Cys-374-Lys-61 was smaller *ca.* 2-2.5Å, and the alteration of the intramonomer εATP-Lys-61 distance was negligible. Using the recently published reconstruction of the F-actin filament, a plausible movement subdomain 2 of actin in response to S1 binding is proposed. Such movement may play an important role in the flexibility and structural dynamics of the filament.

**W-AM-E5**

PERIODIC REPEAT OF CROSS-BRIDGE ATTACHMENT ALONG A SINGLE ACTIN FILAMENT MEASURERD BY AN OPTICAL TWEEZERS PICONEWTON TRANSDUCER. ((Molloy, J.E., Burns, J., & White, D.C.S.)) Department of Biology, University of York, UK

We have measured interactions between single molecules of rabbit myosin subfragment 1 (S1) and rabbit actin filaments with an optical tweezers piconewton transducer. We applied a periodic movement of the thin filament backwards and forwards past the S1 with an amplitude of 100 nm and a velocity of 50 nm.$s^{-1}$. S1 attachments show as upward deflections of the force traces (A). In figure B the actin displacement is plotted against the force; the positions of the cross-bridge attachments are shown by the vertical deflections (arrowed). Such deflections occur at regular intervals in these very preliminary experiments at intervals of about 36-40 nm, close to the helical pitch of the thin filament of 38.5 nm.

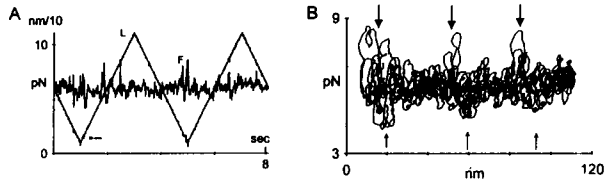


Supported by BBSRC and the Royal Society

**W-AM-E6**

SINGLE MOLECULAR MYOSIN MECHANICS. ((A.D. Mehta, J. T. Finer, J. A. Spudich)) Dept of Biochemistry , Stanford Univ. School of Medicine, Stanford CA 94305

Our research involves the mechanical properties of a single myosin power stroke. To enable direct measurements of the relevant parameters, a new *in vitro* assay has been developed using optical trapping technology which allows nondestructive manipulation of micron-sized dielectric particles. Single actin filaments are chemically attached to latex beads and maneuvered into close proximity of coverslip-bound heavy meromyosin molecules. A quadrant photodetector is used to monitor nanometer displacements of the trapped bead with millisecond resolution. A relatively weak trap is used to establish low load conditions, under which myosin heads are observed to produce discrete, stepwise movements of actin. Active electronic feedback is utilized to increase trap stiffness and enable measurement of picoNewton forces exerted by myosin under near-isometric conditions. Our initial studies have shown that these isolated forces and displacements are consistent with predictions of the conventional swinging crossbridge model of muscle contraction. We have extended these studies to measure forces generated at various points during the power stroke. Additionally, we have examined strain dependent kinetics of single molecular interactions.

**W-AM-E7**

MUSCLE MYOSINS DIFFER IN THEIR *IN VITRO* FORCE GENERATING CAPACITIES. ((P. Van Buren, D. Harris, N. Alpert & D. Warshaw)) Mol. Physiol. & Biophys., Univ. of Vermont, Burlington, VT 05405. (Spon. by J. Peterson)

The average isometric force per cross bridge (F) generated by muscle myosin isozymes may vary by 5 fold. This estimated range was obtained by *in vitro* motility experiments conducted on mixtures of various myosins. The following rank order in F was observed using this indirect approach: F(smooth) > F(skeletal) = F(V3 cardiac) > F(V1 cardiac) (Harris et al., 1994). To directly assess these myosins' force generation, a fluorescently labeled actin filament was attached to an ultra compliant (50-200 nm/pN) glass microneedle and allowed to engage as few as 50 myosins anchored to a motility surface. Average isometric force per cross bridge was calculated from the microneedle deflection. Using this approach, we have previously determined that F(smooth) = 3 x F(skeletal) (Van Buren et al., 1994). We have now determined that F(V3 cardiac) does not differ from F(skeletal) and is 1.6 x F(V1 cardiac). This confirms our earlier indirect estimates and rank ordering. The difference between F(V3 cardiac) and F(V1 cardiac) is intriguing given the 93% sequence identity between the V1 and V3 cardiac myosin isoforms since molecular differences are concentrated in several important regions (e.g. the ATP binding pocket and actin binding domain) (McNally et al., 1989). Mutagenesis coupled with single motor mechanics may help determine the functional significance of these structural regions to myosin's force production and why force differs for various myosin isozymes.

**W-AM-E8**

STEP SIZE AND UNITARY FORCE MEASURED IN BOTH SMOOTH AND SKELETAL MUSCLE MYOSIN ((William H. Guilford, Junru Wu, Guy Kennedy and David M. Warshaw)) University of Vermont, Burlington, VT 05405

Our lab has previously compared the average force generating capabilities of smooth and skeletal muscle myosin in the *in vitro* motility assay and found that smooth muscle myosin generates greater average force per crossbridge (VanBuren *et al.*, 1994; Harris *et al.*, 1994). At the level of a single myosin, the greater average force per crossbridge may be reflected in the size, duration or kinetics of single motion and force generating steps. To test this hypothesis, we have constructed a laser optical trap similar to that of Finer *et al.* (1994) to measure the step size and unitary force from single smooth and skeletal muscle myosin molecules. A fluorescently labeled actin filament was suspended between two NEM-myosin-coated microspheres in independent traps, and allowed to interact with single myosin molecules in an *in vitro* motility assay. Detection of step displacements was limited by Brownian noise to about 3 nm. At 10 μm ATP, the smallest single step displacements observed in skeletal muscle myosin were 11 nm, in agreement with the measurements of Finer *et al.* (1994) in HMM. In contrast, smooth muscle myosin generated smaller single steps of 6 nm under similar loads. Larger events, consisting of multiples of these single step sizes, were observed in both isoforms. Step displacements for smooth muscle myosin averaged 5 times greater in duration than skeletal muscle myosin. The longer event durations for smooth muscle myosin are consistent with the slower kinetics of the crossbridge cycle based on biochemical and physiological evidence. These results suggest significant mechanical differences between smooth and skeletal muscle myosins. We have implemented feedback on our laser optical trap with the goal of comparing unitary force generation of smooth and skeletal muscle myosins.

W-AM-E9

**FORCE MEASUREMENTS IN MYOFIBRILS FROM FROG CARDIAC AND FAST SKELETAL MUSCLE.** ((F. Colomo, N. Piroddi, C. Poggesi & C. Tesi)) Dipartimento di Scienze Fisiologiche, Universitá di Firenze, Italy. (Spon. by G. Cecchi).

Experiments were performed using single myofibrils or thin bundles of few myofibrils 50-250 μm long, prepared by (i) homogenization of frog glycerinated hindlimb muscles, and (ii) chemical skinning of single frog atrial myocytes. The preparations were mounted horizontally between the lever arms of a force transducer and a length control motor (Colomo et al. J. Physiol. 1994, 475.2, 347-350) in a temperature controlled trough filled with relaxing solution (pCa 8, temperature 15 °C). The sarcomere length was set just above the slack length (2.10-2.20 μm). Maximal activation of the preparations was induced by highly localised application of a pCa 4.75 solution injected through a micropipette connected, via an electrovalve, to a pressure reservoir. In the skeletal myofibrils, the absolute value of active force depended upon the number of myofibrils in the preparation, ranging from 0.4-0.6 μN for a single myofibril to values 2-3 times higher in bundles of 2-3 myofibrils. The values for maximal force normalized for the cross sectional area of the preparations provided an average tension value of 0.43 ± 0.05 N/mm$^2$ (mean ± SE n=10), that is in reasonable agreement with the tension values measured in intact frog skeletal muscle fibres during the plateau of tetanic contractions. In 34 frog atrial myocytes the maximal isometric force ranged from 0.5 to 2.5 μN and averaged 1.49 ± 0.13 μN. Since frog atrial cells contain only few myofibrils (1 to 5), the force values found suggest that the active force produced by a single frog cardiac myofibril is close to 0.5 μN and does not differ significantly from that developed by single frog skeletal myofibrils.

## CATALYTIC RNA: MECHANISM AND STRUCTURE

W-AM-SymII-1

THREE-DIMENSIONAL STRUCTURE OF A HAMMERHEAD RIBOZYME, Heinz W. Pley, Kevin M. Flaherty, and , David B. McKay, Stanford University School of Medicine, Stanford, CA 94305.

The hammerhead ribozyme is a small catalytic RNA motif made up of three base-paired stems and a core of highly conserved, non-complimentary nucleotides that are essential for catalysis. The x-ray crystallographic structure of a hammerhead RNA-DNA, ribozyme-inhibitor complex has been solved to 2.6 Angstrom resolution. The base-paired stems are A-form helices. The core has two structural domains. The first domain, formed by the sequence 5'-CUGA following stem I, is a sharp turn that is identical in structure to the uridine turn of tRNA. The second domain is a non-Watson Crick duplex of sequence $^{5'\text{-U-G-A-3'}}_{3'\text{-A-A-G-5'}}$. Anomalous scattering measurements with $Mn^{2+}$ and $Cd^{2+}$ identify a divalent ion binding site in the second domain. The phosphodiester backbone of the DNA inhibitor strand is splayed at the phosphate 5' to the cleavage site. The structure suggests that the ribozyme facilitates cleavage by destabilizing both the phosphodiester linkage at the cleavage site and the linkage 5' to it.

W-AM-SymII-2

MECHANISMS OF RNA CATALYSIS BY GROUP II INTRONS. ((Anna Marie Pyle, William J. Michels, Kevin Chin, Justin Green and Dana Abramovitz)) Department of Biochemistry and Molecular Biophysics, Columbia University, New York, NY 10032.

Group II introns are self-splicing RNAs essential for the processing of many organellar genes in plants, fungi and other organisms. They have also been widely accepted as models for the catalytic center of the eukaryotic spliceosome. Despite their apparent lack of extended tertiary structure, groupII introns contain functionalities for the catalysis of many different chemical transformations. We have divided this large RNA into several different ribozyme constructs, in order to focus on the mechanism and active-site structure important for catalysis of individual reactions related to the first step of self-splicing. Few base-pairing interactions stabilize the tertiary structure of this RNA and we have observed that catalytically essential Domain 5, when added in trans to different ribozyme constructs, binds tightly through a network of specific 2'-hydroxyl groups. Similarly, other subdomains of the intron nest into active sites through backbone-mediated interactions. Group II intron active sites can catalyze attack on RNA through either hydrolysis or transesterification (branching) and both pathways are always in direct competition. We have constructed ribozymes to examine both pathways, finding that the internal equilibrium of branching causes it to proceed more readily in reverse than in the forward direction. Branching proceeds through stochastic sampling of a conformation that rapidly catalyzes transesterification. Both pathways are observed to compete in the full-splicing reaction of group II introns. We show that hydrolytic and branching mechanisms are both important to the function of group II introns and the preponderance of either pathway can be modulated by addition of proteins and other reaction cofactors.

W-AM-SymII-3

RNA-CATALYZED AMINOACYL-RNA SYNTHESIS. ((M. Yarus)) Univ. of Colorado.

W-AM-SymII-4

STRUCTURAL ELEMENTS IN A HAIRPIN RIBOZYME, ((Ignacio Tinoco, Jr., Zhuoping Cai, and Jeffrey Kieft)) Department of Chemistry, University of California, Berkeley, and Structural Biology Division, Lawrence Berkeley Laboratory, Berkeley, CA 94720.

We are studying the structure of a hairpin ribozyme derived from the minus strand of tobacco ring spot virus satellite RNA. This ribozyme has been engineered to specifically cleave the HIV-1 RNA. The catalytically active system contains a 49-nucleotide ribozyme which specifically cleaves and ligates a 14-nucleotide substrate. The secondary structure of the ribozyme-substrate complex consists of four short helices separated by two internal loops (loops A and B). We are using NMR to determine the high resolution structures of the two loops.

The substrate plus substrate-binding site of 28 nucleotides contains a symmetric internal loop of 8 nucleotides (loop A) with its flanking helices. Isotope-edited 2D and 3D NMR experiments on selectively $^{13}$C-labeled molecules were used to facilitate resonance assignments. The cleavage site is at a 5'-CpG-3' step in one strand of loop A. NOEs between groups on either side of the cytidine, plus its pure 2'-endo conformation, indicate that the cytidine is bulged out. The aromatic protons of the cytosine and the H1' protons of the adjacent G•C base pair are broadened, indicating millisecond dynamics for this part of the loop.

The 35-nucleotide fragment can fold into an asymmetric internal loop of 16 nucleotides (loop B). Photo-crosslinking studies of Butcher and Burke [*Biochemistry* 33, 992 (1994)] suggest that loop B is similar to loop E of eukaryotic 5S RNAs [Wimberly et al., *Biochemistry* 32, 1078 (1993)].

W-AM-F1

## NMR INVESTIGATION OF THE EFFECTIVE SHAPE OF PHOSPHOLIPID HYDROCARBON CHAINS

((K. Gawrisch, L.L. Holte)) NIAAA, NIH, Bethesda, MD 20892

$^2$H NMR spectra of perdeuterated hydrocarbon chains were analyzed in terms of order parameter profiles. The profiles are sensitive to unsaturation, lipid headgroup structure, and interactions at the lipid water interface (proteins, ions, solvents). The measurements indicated high chain order in the first half of the chain and rapidly decreasing order towards the terminal methyl group in the second half of the chain. This decrease in order is related to an increased deflection of chain segments from the bilayer normal. Hydrocarbon chains tumble in a cone-shaped volume. However, by definition, in a lamellar arrangement, lipids occupy a cylindrical space if membrane curvature can be neglected. This is an apparent contradiction. Consequences for packing of lipid hydrocarbon chains and for the structure of membranes at the lipid water interface will be discussed. We suggest that there is a link between permeation of solvent molecules and protein sidechains into lipid bilayers and changes of the effective shape of lipid hydrocarbon chains as measured by NMR.

W-AM-F2

## CRYO-ELECTRON MICROSCOPY OF PHOSPHOLIPID VESICLES.

(( W. Helfrich*, B. Klösgen*,)) FU Berlin, FB Physik, *: Inst.f. Theoretische Physik, *: Inst. f. Experimentalphysik, Arnimallee 14, D-14195 Berlin, Germany.

Among the electron microscopic techniques available to investigate lipid structures cryo-TEM is the one believed to be the most non-destructive method. Though freezing artefacts have been shown to induce tensions in membranes and thus may change the membrane structure and vesicle shapes, the method can be used successfully if it is combined and controlled with other methods ( as x-ray microscopy, e.g. ). Here we present micrographs obtained from small (mostly ) unilamellar vesicles of POPC in pure water. Our aim was to increase the number of vesicles that are rather big (up to 300nm of mean diameter) and at low mechanical tension as well. Under that condition, non-spherical shapes of vesicles can be prepared and maintained despite of the shock-freezing artefacts. In few cases, induced membrane adhesion of a stressed vesicle and a more relaxed one could be preserved despite of the cryo-preparation. Some vesicle contours exhibit deviations from a smooth appearance; sometimes there is the vage impression of a contrast modulation all over a vesicle membrane. Both effects may be interpreted as the result of a membrane superstructure in the liquid phase. Stable folds observed in lipid vesicles with x-ray microcopy in wet sample chambers at normal conditions also support that idea.

W-AM-F3

## 2D-EXCHANGE DEUTERIUM-NMR EXPERIMENTS OF PHOSPHOLIPID BILAYERS ON A SPHERICAL SOLID SUPPORT

((C. Dolainsky[1], M. Unger[1], M. Bloom[2], T. M. Bayerl[3])) [1]Technische Universität München, Physik Department E22, D-85747 Garching,Germany, [2]University of British Columbia, Dept. of Physics, V6T 2A6, Vancouver, Canada, [3]Universität Würzburg, Physikalisches Institut EP-V, D-97047 Würzburg, Germany

Bilayers of 1-palmitoyl-2-oleoyl-sn-glycero-3-phosphocholine (POPC) on a spherical solid support consisting of silica beads are studied by two-dimensional exchange deuterium NMR (2D-exchange NMR) at two hydration states of the bilayer and at mixing times in the range 1-8 ms. The spectra obtained were analysed in terms of a solution of the diffusion equation of molecules diffusing on the surface of a sphere with a radius corresponding to that of the solid support. This procedure gives a jump angle distribution function of the lipids for a fixed mixing time. The well defined geometry of the sample enables us to compare the experimental results with those obtained by a random walk simulation assuming that solely diffusional jumps of the POPC molecules contribute to the 2D-exchange NMR spectra during the mixing time. We reached an excellent agreement between the results obtained by experiment, simulation and by the numerical calculation based on the diffusion equation. These results provide strong evidence that lateral diffusion of lipids is by far the most important mechanism which determines the spectral evolution in 2D-exchange NMR spectroscopy of curved lipid bilayers. It is concluded that future applications of the 2D-exchange NMR method may provide valuable insight in the topology and the slow motion dynamics of biological membranes.

W-AM-F4

## BINDING OF PROTEINS TO MIXED LIPID MEMBRANES

((D.Marsh and T.Heimburg)) Abt.01, Max-Planck Institut für biophysikalische Chemie, 37077 Göttingen, Germany

An analytical expression for the binding isotherms of peripheral proteins to charged lipid membranes was derived. The theoretical description was extended to the binding of proteins to mixtures of charged and uncharged lipids, allowing for binding-induced inhomogeneities in the mixed lipid membranes. The model is based on a statistical thermodynamic description that includes the electrostatic free energy (deduced from the Gouy-Chapman theory) and distributional free energy of proteins on the lipid surface. Also included are possible attractive or repulsive interactions between ligands as well as preferable binding to one lipid species. Dependent on the ionic strength, the binding of proteins can be calculated in the full range of ligand filling of the surface. In the absence of ligand-ligand interactions the isotherms are controlled by only three parameters: the effective charge of the protein Z, the intrinsic binding constant $K_0$, and the size of the ligand. All three parameters can be obtained from independent experiments.

To put the presented model to the test, the binding of the peripheral globular protein cytochrome c to mixed lipid membranes, consisting of dioleoyl phosphatidylglycerol and dioleoyl phosphatidylcholine, was investigated at various salt concentrations and lipid ratios. The binding of cytochrome c to those membranes could only then consistently be described, if binding induced inhomogeneities in the lipid distribution were assumed. This leads to an increase of the charged lipid concentration in the protein binding site.

W-AM-F5

## INTERACTION OF MELITTIN WITH LIPID MEMBRANES.

((S. Ohki, D.K. Sukumaran and K. Arnold*)) Department of Biophysical Sciences, SUNY at Buffalo, Buffalo, NY 14214 and Institute of Biophysics, University of Leipzig, Leipzig, Germany*.

Interaction of melittin with lipid membranes was studied with respect to its adsorption onto the membranes, and its effects on membrane leakage and fusion. Measurements of lipid vesicle electrophoretic mobility and lipid monolayer expansion due to the presence of melittin in the solution indicated that melittin was adsorbed onto a phosphatidylserine membrane several times more than a phosphatidylcholine membrane. However, it was observed by fluorescence studies that the neutral lipid membrane is more susceptible to membrane leakage and fusion by melittin than the charged membrane. Thus, it was deduced that melittin molecule tends to stay out on the surface of the acidic lipid membrane, whereas it is adsorbed more into the membrane hydrocarbon core for the electrically neutral lipid membrane. This was also confirmed from the study on the interaction of the above two lipid membrane systems in the presence of polyethylene glycol (PEG). The same concentration of melittin in the solution induced a greater extent of fusion of phosphatidylcholine membranes than phosphatidylserine membranes, both of which are adhered at a same extent by PEG.

W-AM-F6

## THE PROLAMELLAR BODY AS A CUBIC CYTOMEMBRANE WITH DOUBLE DIAMOND SYMMETRY: A PUTATIVE PHOTON BLOCKER.

((Yuqing Guo, Mark Mieczkowski and Tomas Landh)) Department of Biomaterials, State University of New York at Buffalo, Buffalo, NY 14214

The prolamellar body (PLB) is a three-dimensional periodic membrane structure formed by the chloroplasts of etiolated leaves in higher plants. Direct comparison of published TEM micrographs of the PLB and computer-simulated projections of periodic cubic surfaces (PCS) shows that PLB is described by the double diamond (D-based) PCS of space group 224 [Landh and Mieczkowski, submitted to *J. Ultrastruct. Res.*]. The structure (symmetry) of the PLB is invariant among species, despite divergent membrane compositions, while the lattice size is observed to vary considerably. In recent studies of "photonic crystals", it was determined that dielectric spheres arranged in the diamond structure possess a full photonic band gap [Ho *et al.* (1990) *Phys. Rev. Lett.* **65**, 3152-3155]. This existence of a full band gap in photonic crystals having the same space group 224 as the PLB has allowed us to hypothesize a possible structure/function relationship within the PLB: the trapping of photons. Experiments with various materials/structures examining this hypothesis as well as further theoretical work to investigate initial steps in the photosynthesis process are in progress.

**W-AM-F7**

**THERMOSENSITIVE LIPOSOMES: EXTRAVASATION AND RELEASE OF CONTENTS IN TUMOR MICROVASCULAR NETWORKS.** ((M.H. Gaber*, N.Z. Wu**, K. Hong*, S-K. Huang***, M.W. Dewhirst**, and D. Papahadjopoulos*)) *CRI, UCSF, San Francisco, CA 94143, **Dept of Rad. Onc., Duke Univ. Med. Ctr., Durham, NC 27710, ***LTI, Menlo Park, CA 94025

We have used *in vivo* fluorescence video microscopy to measure the extravasation of thermosensitive sterically stabilized liposomes (TSSL) as well as the release of their contents in a rat skin flap window chamber containing a vascularized mammary adenocarcinoma at 34 , 42 and 45°C. The image of a tissue area containing multiple blood vessels was recorded via a SIT camera immediately before, and for 2h after i.v. injection of liposomes surface-labeled with Rhodamine-PE ( Rh-PE ) and liposomes containing Doxorubicin (Dox) at self-quenching concentrations. The light intensity of the entire tissue area was measured at 34°C for 1h and at 42°C or 45°C also for 1h. The intensity of Rh-PE for the TSSL in the interstitial space (representing extravasated liposomes) was very low during the first hour (before heating starts) and increased up to 47 times its level, when the tumor was heated at 42°C or 45°C for 1h. The intensity of the liposome contents (Dox) in the interstitial space was negligible during the first hour, and increased up to 38 and 76 times its level (indicating release), when the tumor was heated at 42°C and 45°C for 1h, respectively. A similar increase in liposome extravasation was seen with non-thermosensitive liposomes, but no significant release of Dox occured when the tumor was heated to 45°C for 1h. Our data suggest that hyperthermia can be used to selectively enhance both the delivery and the rate of release of drugs from (thermosensitive) liposomes to targeted tissues.

**W-AM-F8**

ELECTROCHEMISTRY OF THE ELECTRODE-TISSUE INTERFACE: *IN SITU* CYCLIC VOLTAMMETRY OF RUTHENIUM(III) HEXAMMINE [$Ru(NH_3)_6^{3+}$] AS A REDOX PROBE IN THE LIVING MAMMALIAN HEART. ((Marc Ovadia[a], Mark H. Schoenfisch[c], Margaret Levy[b], Jeanne E. Pemberton[c])) [a]North Shore Univ. Hosp. (Cornell Univ. Medical Coll.), Manhasset, NY 11030, [b]Univ. Heart Ctr. and [c]Dept. of Chemistry, Univ. of AZ, Tucson, AZ 85721

Electrochemical characteristics of the cardiac electrode-tissue interface relevant to active-fixation pacing electrodes have been determined using *in situ* cyclic voltammetry of $Ru(NH_3)_6^{3+/2+}$ (reversible reduction and oxidation) in the living heart in order to determine the resistivity of myocardium. Tracheostomy and median sternotomy were performed in 24 adult Sprague rats. The aorta was cannulated *in situ* and perfused with Ca-free oxygenated buffer. Cyclic voltammetry was performed using a two-electrode arrangement with a platinum wire (0.37 mm dia, 2-6 mm exposed) working electrode in ventricular myocardium and a silver quasi-reference electrode 8-10 mm away. Resistance was measured using square wave pulses fit to a single-order exponential RC decay. As an alternate measure of interfacial resistance, $Ru(NH_3)_6^{3+}$ (0.5 to 5 mM) was perfused followed by cyclic voltammetry at four scan rates with measurement of $\Delta E_p$, peak and limiting current, and shape. **Results:** Three types of curve morphology were identified corresponding to presence or absence of bulk fluid movement at the interface, and electrode-myocardial vs. electrode-cavitary contact in the latter. $O_2$ removal by specimen at the electrode tissue interface appeared to corroborate electrode position in metabolically active myocardium. In electrode-myocardial interfaces with no bulk fluid movement, $\Delta E_p$ was measured for the $Ru(NH_3)_6^{3+/2+}$ redox process, and found to be 2 ($\pm$ 0.1) x $10^2$ mV, indicating a resistance of 6 ($\pm$ 1) x $10^2$ $\Omega$. All other interface types manifested electrode-solution and not electrode-myocardial tissue interfacial characteristics with no rectification. **Conclusions:** Cyclic voltammetric measurements relevant to active-fixation pacing electrodes can be performed in the living heart *in situ*. Both measures of myocardial resistance were consistent with 6 x $10^2$ $\Omega$ between two electrodes 8-10 mm apart. These are the first such electrochemical measurements in the living mammalian heart and contradict previously reported measures of resistance in implanted pacemakers. Previous measurement systems may suffer from parallel current pathways through liquid or metabolically inactive tissue (e.g. edema,scar, or inexcitable muscle).

**W-AM-F9** *(See Th-Pos378)*

## CHLORIDE CHANNELS

**W-AM-G1**

THE ROLE OF NBF2 IN GATING THE CYSTIC FIBROSIS TRANSMEMBRANE CONDUCTANCE REGULATOR (CFTR) CHLORIDE CHANNEL. (( Kevin L. Gunderson and Ron R. Kopito)) Biophysics Program and Dept. of Biological Sciences, Stanford University, Stanford, CA 94305-5020. (Spon. by P. Hanawalt)

CFTR is a chloride channel whose gating is controlled by a cycle of ATP hydrolysis through interaction with the two nucleotide binding folds (NBFs). The precise relation between ATP hydrolysis and gating by the two NBFs is poorly understood. In this study, we investigate the role of the NBF2 in CFTR gating. Site-directed mutants of the P-loop region (Walker A motiff) in NBF2, produced channels exhibiting two distinct gating phenotypes upon reconstitution into planar bilayers. Mutations of the highly conserved P-loop lysine residue (K1250) resulted in a MgATP dependent gating phenotype characterized by prolonged open bursts (> 1 min.). This gating phenotype contrasts with that seen in wild type CFTR in which the mean open burst time is about 300 ms. Furthermore, the prolonged open bursts of the K1250 mutants resemble those seen with wildtype CFTR in the presence of non-hydrolyzable compounds like AMP-PNP or PPi, suggesting that attenuation of the hydrolysis rate at NBF2 leads to prolonged open bursts. A second gating phenotype was exhibited by a P-loop mutation expected to be deficient in nucleotide binding (G1247D,G1249E). This mutant responded poorly to MgATP, and was not susceptable to being "locked" open by PPi. This observation suggests that binding of MgATP to NBF2 increases the opening rate of the CFTR chloride channel. Finally, to establish whether NBF2 functions differently than NBF1, we examined the NBF1 P-loop lysine mutant, K464A, homologous to K1250A. In contrast to the K1250A mutant, the K464A mutant did not exhibit any prolonged "locked" open bursts in the presence of MgATP, but responded poorly to ATP. These results suggest a minimal model for CFTR gating in which NBF2 plays a key role in both opening and closing the channel. In particular, ATP binding at NBF2 facilitates channel opening, whereas ATP hydrolysis at NBF2 leads to channel closure.

**W-AM-G2**

THE CFTR IS REGULATED BY THREE FUNCTIONALLY DISTINCT PHOSPHATASES. ((Horst Fischer, Beate Illek and Terry E. Machen)) University of California, Berkeley, CA 94720.

The cystic fibrosis transmembrane conductance regulator (CFTR) is the epithelial Cl channel regulated by phosphorylation by kinases and phosphatases. We have investigated fibroblasts stably transfected with the CFTR with the patch clamp technique in conjunction with current noise analysis, and transepithelial Cl currents in basolaterally α-toxin permeabilized HT-29/B6 epithelia. The phosphatase inhibitors calyculin A (blocks PP1), okadaic acid (blocks PP2A), and deltamethrin (blocks PP2B) are highly specific for the respective phosphatases when used in picomolar or nanomolar concentrations. Calyculin A or okadaic acid alone did not stimulate Cl currents in cell-attached patches, whole-cell recordings or transepithelial recordings. Cyclic-AMP or forskolin stimulated CFTR-mediated Cl currents in all mentioned recording conditions. Addition of calyculin A to cAMP-stimulated cells further increased currents, while okadaic acid inhibited currents. In contrast to the other inhibitors, deltamethrin stimulated CFTR channels on its own in whole-cell and cell-attached recordings. Current fluctuation analysis showed that corner frequencies were unchanged by deltamethrin or okadaic acid when compared to forskolin stimulations, while calyculin reduced corner frequencies significantly. From this we propose a model in which CFTR's opening is regulated by three phosphorylations: (i) PP2B controls a key initial phosphorylation for channel activation, (ii) PP2A regulates a subsequent phosphorylation of an inhibitory site, and (iii) the PP1 dependent phosphorylation immediately precedes the ATP-dependent opening of the channel.
Supported by the Cystic Fibrosis Foundation and the Cystic Fibrosis Research Inc.

**W-AM-G3**

ACTIVATION OF CFTR CHLORIDE CHANNELS BY FORSKOLIN AND GENISTEIN. ((T.-C. Hwang and E. M. Price)) Department of Physiology and School of Veterinary Medicine, Dalton Cardiovascular Research Center, University of Missouri-Columbia, Columbia, MO 65211.

Effects of forskolin, an activator of adenylate cyclase, and genistein, a tyrosin kinase inhibitor, on CFTR $Cl^-$ channels were studied in NIH 3T3 cells stably expressing recombinant CFTR by recording channel currents in cell-attached patches. Pipette solutions contained 140 mM NMGCl and the bath solution contained 145 KCl. Channel activity can be elicited in 30 s by bath application of forskolin (10 μM) or genistein (50 μM). Channel activity was diminished following removal of forskolin or genistein. The single channel I-V relationship showed outward rectification with a reversal potential around -5 mV pipette potential ($V_p$). Single channel conductance, calculated by linear regression over the negative $V_p$, is ~10pS. In patches containing multiple channels, bath application of either chemical activated outward currents at negative $V_p$ while inward current at positive $V_p$, consistent with the single channel results. Although CFTR channel activity can persist for tens of minutes in the presence of activators, it disappeared immediately upon excision into bath solution containing neither ATP nor protein kinase A (PKA). Effects of ATP and PKA on CFTR channels in excised patches are currently under investigation. Our results confirmed those of Illek et al., (Am. J. Physiol. 1994. in press). Since we observed occasional channel opening in the absence of any agonists, suggesting possible significant basal phosphorylation of the CFTR channels, it remained to be determined whether tyrosin kinase is involved directly in the regulation of the channels or serine/threonine phosphatases are affected by genistein. Supported by AHA, Missouri Affiliate.

**W-AM-G4**

HUMAN HEART CELLS LACK CFTR-LIKE CHLORIDE CURRENT BUT EXPRESS A SWELLING-INDUCED CHLORIDE CURRENT THAT IS STIMULATED BY FORSKOLIN. ((S. Sorota)) Dept. of Pharmacology, Columbia University, New York, NY.

Myocytes were isolated from pieces of human right atrial appendage. Whole cell patch clamp was used. Steady-state currents were measured with hyperpolarizing ramps (-15 mV/sec). Peak net inward currents during voltage steps from -50 mV to +5 mV were used to look for modulation of L-type calcium current. Forskolin (FOR, 10 μM) was used to look for a CFTR-like chloride current. No FOR-induced steady-state current was found in any of 15 cells (6 patients). FOR increased peak net inward current in all cells. Swelling with osmotic stress induced an outwardly rectifying steady-state current ($I_{swell}$) with a reversal potential close to $E_{Cl}$. In hypotonic solutions, FOR caused an increase in $I_{swell}$ (4 of 4 cells, 2 patients). The effect of FOR washed out. The reversal potential of $I_{swell}$ was sensitive to the chloride concentration in the patch electrode. Outward $I_{swell}$ was blocked by 150 μM DIDS. Human ventricle cells were isolated from 5 cadiac transplant patients. No FOR-induced steady-state current was found in any of 17 cells. FOR increased peak net inward current in every cell. Guinea pig ventricle cells were prepared using the same lot of collagenase used for isolation of human cells. A DIDS-insensitive FOR-stimulated chloride current was seen in 5 of 6 guinea pig cells. In 8 of 8 human ventricle cells, exposure to hypotonic solution activated an outward $I_{swell}$ at positive voltages. In 4 of 4 cells, FOR increased the amplitude of this outward current. The FOR-stimulated outward $I_{swell}$ was inhibited by DIDS. In spite of reports that human heart cells contain mRNA for CFTR-like chloride channels, the present results suggest that there are not significant amounts of these channels in human atrium or failing ventricle. Human heart cells do express a swelling-induced chloride current that can be stimulated by forskolin. Inhibition of outward currents by DIDS can be used to discriminate between the swelling-induced chloride currents and the CFTR-like chloride current. (Supported by an Investigatorship and a Grant-in-Aid from the American Heart Association, New York City Affiliate).

W-AM-G5

## $I_{CLN}$ THE SWELLING INDUCED CHLORIDE CHANNEL CLONED FROM EPITHELIAL CELLS

(( Markus Paulmichl, Martin Gschwentner, Ulrich O. Nagl, Hannes Fürst#, Ewald Wöll§, Andreas Laich, Erwin Rovan#, Alex Susanna, Andrew Dobson, Andreas Schmarda, Germar Pinggera, Markus Leitinger )) Department of Physiology, Fritz-Pregl-Str. 3, § Department of Internal Medicine, Anich-Str. 35, University of Innsbruck, A-6020 Innsbruck, Austria and # Department of Zoology, University of Salzburg, A-5020 Salzburg, Austria, Europe.

The activation of chloride channels is one of the initial steps to reduce the cellular volume after swelling. The simultaneous stimulation of potassium channels enables the cells to lose potassium and chloride together with water and therefore reduce their volume. The chloride channels involved in regulatory volume decrease of fibroblasts belong to a specialized class of proteins named $I_{Cln}$ initially cloned from a kidney cell-line. $I_{Cln}$ expressed in *Xenopus laevis* oocytes is sensitive to the extracellular addition of the chloride channel blocker NPPB and nucleotides. Similarly sensitive are endogenous $I_{Cln}$ chloride channels activated after swelling of NIH 3T3 fibroblasts. These channels are, in addition, sensitive to phenol derivatives and nucleoside analogues added to the extracellular solutions. Using immunogold silver staining (IGSS) in combination with a laser scanning microscope $I_{Cln}$ can be exclusively localized in the brush border membrane of proximal tubule epithelial cells. In the cells of the kidney medulla and in fibroblasts the $I_{Cln}$ protein can be localized both in the cell membrane as well as in the cytosolic compartment. In fibroblasts the water soluble cytosolic component of $I_{Cln}$ can selectively be 'driven' into the membrane after exposing the cells to hypotonic stress. The experiments show that $I_{Cln}$ is the swelling activated chloride channel itself.

W-AM-G6

## CHLORIDE CURRENTS IN MOUSE INNER MEDULLARY COLLECTING DUCT (IMCD) CELLS.

((M. Shindo, N.L. Simmons & M.A. Gray.)) Dept. Physiological Sciences, University Medical School, Newcastle upon Tyne. NE2 4HH. U.K.

The IMCD plays an important role in determining final urinary salt composition. Recent work (1) has shown that IMCD cells express mRNA for two Cl channel proteins, CFTR and ClC-2. Here we show, using standard whole-cell current (WCC) recordings, that mouse IMCD-3 cells possess two types of Cl conductances, which can be distinguished by different biophysical properties and sensitivity to pharmacological agents. Cells were bathed in a standard Na-rich solution and the pipette contained predominantly TEACl. In 30 % of cells WCC were voltage-independent over the range ± 100 mV, with a linear I/V plot, and a current density of 67 ± 6.7 and 66 ± 6.7 pA/pF (n=38) at ± 60 mV respectively. In 46 % of cells WCC were slightly time and voltage-dependent, with an outwardly-rectifying I/V plot. WCC density at ± 60 mV was 76 ± 6.2 and 49 ± 4.0 pA/pF (n=58). The two currents could be distinguished by marked differences in permeability to $ClO_4$ (relative to Cl) and their sensitivity to block by NPPB, flufenamate and glibenclamide (0.1 mM). Both conductances were largely insensitive to block by DIDS (0.5 mM). Increases in intracellular cAMP or Ca had no effect on either conductance. Our data provide the first demonstration of Cl currents in IMCD cells. The properties of the linear current are similar to CFTR, and suggest that expression of CFTR in these cells is likely to have an important role to play in IMCD tubular function.

(1) Morales et al. (1994) FASEB J. 8. a294 1697.

Funded by a University Fellowship to MS

W-AM-G7

## $Cl^-$-DEPENDENT GATING OF THE VOLTAGE-DEPENDENT CHLORIDE CHANNEL, ClC-0

((*U. Ludewig, M. Pusch, & T.J. Jentsch*)) ZMNH, Hamburg University, D-20246 Hamburg, Germany

$Cl^-$-channels of the ClC-family are important for the control of membrane excitability, cell volume regulation, and possibly transepithelial transport. Although lacking the typical voltage-sensor found in cation channels, gating of ClC channels is clearly voltage-dependent. The *Torpedo* electric organ $Cl^-$-channel, ClC-0, has a "slow" gate operating on both protochannels of the double-barreled channel simultaneously, and a "fast" gate acting on single protochannels. We expressed ClC-0 in *Xenopus* oocytes and studied the fast gate in isolation. We found that voltage-dependence and kinetics of fast gating depend on $[Cl^-]_{ext}$. The nominal gating charge remains ~1 throughout. This can be described by a simple model in which the permeating anion acts as the gating charge and facilitates channel opening by binding to a site at the cytoplasmic end of the pore. We identified a highly conserved lysine residue to be important in this process. Eliminating this positive charge changed kinetics, $[Cl^-]_{ext}$-dependence, and halide-selectivity of gating, and altered pore properties such as ion selectivity, channel conductance, and rectification. Thus this mutant strongly suports the model. In addition, mutating this lysine, renders the closed state of WT ClC-0 partially conducting ("leaky closed state") undermining its importance in gating and conductance.

W-AM-G8

## LYSOPHOSPHATIDIC ACID ACTIVATES $Cl^-$ CHANNELS IN RABBIT CORNEAL KERATOCYTES.

((M.A. Watsky)) Department of Physiology and Biophysics, University of Tennessee, Memphis, TN 38163.

Corneal keratocytes reside in the corneal stroma in an inactive state, and are activated to repair injured stroma following corneal trauma. The primary voltage-gated ion channel types found in inactive keratocytes from normal corneas include the delayed rectifier $K^+$ channel and $Na^+$ channels. Activated cells from injured corneas tend to lose most or all of this voltage-gated channel activity. In this study, we used keratocytes from injured corneas to investigate the influence of nature's simplest phospholipid, lysophosphatidic acid (LPA or 1-oleoyl-2-lyso-*sn*-glycero-3-Phosphate) on the ion channel activity of these cells. LPA has been shown to have hormone- and growth factor-like activity in other cell types. Cells were isolated from the corneas of rabbits injured with a liquid nitrogen cooled probe 90 hours prior to the experiment. Whole-cell currents were examined using the amphotericin perforated patch technique. Almost immediately after application of 10 μM LPA, large (up to 2 nA) fast activating outward currents with minimal inactivation were observed. Current amplitude increased with time. The reversal potential of these currents was 0 mV with an internal 145 mM K-methanesulfonate Ringer's and an external 149 mM NaCl Ringer's solution. Currents reversed at positive potentials following addition of 47 mM NaCl Ringer's (sucrose substitution) to the bath. Currents were blocked by the $Cl^-$ channel blockers DIDS, NPPB, DPC, and flufenamic acid. Lysophosphatidylcholine (10 μM ) failed to activate the current. We conclude that LPA activates $Cl^-$ channels in corneal keratocytes from injured corneas. (Supported by NIH grant EY10178).

W-AM-G9

## EFFECT OF pH ON THE GATING PROPERTIES OF A RECOMBINANT HUMAN MUSCLE CHLORIDE CHANNEL.

((Ch.Fahlke, A.L.George, A.Rosenbohm, R.Rüdel)) Dept. of Gen. Physiology, Univ of Ulm, D-89069 Ulm, Dept. of Med, Vanderbilt Univ, Nashville, TN 37232, USA (Spon. A.K. Kleinschmidt)

The $Cl^-$ channel, hClC-1, was stably expressed in HEK 293 cells for the examination of its gating properties by whole-cell recordings. Hyperpolarizing voltage steps from a holding potential of -30 mV elicit deactivating currents that are described by sums of 2 exponentials and a time-independent component. Both time constants are voltage-independent, but vary with $pH_i$, both with pK values < 6.0 ($\tau_{fast}$ for deactivation is 1.0 ms at pH 9.5 and 170.4 ms at pH 5.5). Changes of $pH_e$ do not alter the time constants. The voltage dependence of the relative amplitudes of the fast, slow and constant current components can be fitted with $B^2$, $2B^*$ (1-B) and $(1-B)^2$, respectively, where B denotes Boltzmann distributions. At $pH_e$ < 7.4, the fast and slow current amplitudes are decreased and the constant component is increased; external alkalinization has no effect. The voltage dependence of activation is similar to that of deactivation. Both processes are nicely represented by a model with two voltage sensors controlling a voltage-independent opening or closing rate. The sensors are affected by $pH_i$ and $pH_e$. The voltage independence and the effects of $pH_i$ on the time constants suggest an activation gate at the cytoplasmic side of ClC-1.

**W-AM-H1**

MOLECULAR MECHANISMS UNDERLYING THE MULTI-ION NATURE OF THE cGMP GATED CHANNEL ((F. Sesti*, U.B. Kaupp+, E. Eismann+, M. Nizzari* and V. Torre*)) *Dipartimento di Fisica, Via Dodecaneso 33, Genova, Italy and +Institut fur Biologische Informationsverarbeitung, D-52425 Jülich, Germany

The native cGMP-gated channel from rods of the tiger salamander Ambystoma tigrinum and the cloned cGMP-gated channel from bovine rods (i.e. the wt channel) expressed in Xenopus laevis oocytes were studied in excised patches. When the patch pipette was filled with 110 mM Li+ or Cs+ and the bathing medium contained isoosmotic mixtures of Li+ and Cs+, an anomalous mole fraction effect was observed, both in the native and the wt channel. When glutamate 363 of the wt channel was neutralized to a glutamine the anomalous mole fraction effect with Li+ and Cs+ mixtures was abolished. The outward current carried by Li+ and Na+ in the native and wt channels was half saturated at ionic activities around 200 mM while no saturation was observed in the mutant E363Q for ionic activities below 400 mM. When other charged residues in the pore region between arginine 346 and glutamate 372 were neutralized to glutamine, the mutant channels exhibited an anomalous mole fraction effect and their affinity for Li+ and Na+ was the same as of the wt channel. These results indicate the native and the wt channel are both multi-ion pores and that the multi-ion nature of the wt channel is primarily controlled by glutamate 363 and not by other charged residues in the pore region.

**W-AM-H2**

TRANS-CHANNEL INTERACTIONS BETWEEN EXTERNAL AND INTERNAL BLOCKERS OF A SODIUM CHANNEL. ((Iván C. Sierralta, Gerald W. Zamponi, and Robert J. French)) Dept Med Physiol & Neurosci Res Group, Univ Calgary, 3330 Hospital Dr NW, Calgary, AB, Canada, T2N 4N1.

R13Q (net charge ~+5) is a 22 amino acid peptide derived from μ-conotoxin GIIIA (μCTX) by substitution of glutamine for arginine-13. Externally applied μCTX, and most of its derivatives, cause discrete, all-or-none block of single skeletal-muscle Na channels, with 1:1 stoichiometry. In contrast, R13Q blocks incompletely, inducing discrete events, of a few seconds duration, having 25-30% of the normal single channel amplitude. (Becker et al., 1992, *Biochemistry* 31: 8229). We have studied block of both the unbound and R13Q-bound channel by the cytoplasmic blocker, diethylammonium (DEA), whose action is enhanced by increasing depolarization. DEA rapidly blocks the open-channel, reducing the apparent single channel amplitude. The fractional block, $f_b$, was reduced at all voltages, V, when an R13Q molecule was concommittantly bound, leading to a 25 mV positive shift of a plot of $f_b$ vs V. The slope of this plot was unchanged, indicating that DEA bound to the same site, about 50% of the way through the transmembrane voltage, regardless of whether R13Q was bound or not. A small increase (~15%) in $IC_{50}$ for R13Q block, when DEA (24 mM) was present, suggests reciprocal inhibition between the two blockers. Our data are consistent with an electrostatic repulsion between cationic blockers that bind to the channel from opposite ends.

**W-AM-H3**

MOLECULAR DETERMINANTS OF Na CHANNEL BLOCK BY ANTICONVULSANT AND ANTIARRHYTHMIC DRUGS. ((D.S. Ragsdale, J.C. McPhee, T. Scheuer, W.A. Catterall)) Dept. of Pharmacology, SJ-30, U. of Washington, Seattle WA 98195.

Local anesthetic, anticonvulsant and cardiac antiarrhythmic drugs block ionic currents through voltage-gated Na channels with complex voltage- and frequency-dependent properties that are important for their therapeutic action and reflect differential drug binding to the resting, open and inactivated channel states. Using site-directed mutagenesis and functional expression in *Xenopus* oocytes, we have identified residues in the IVS6 transmembrane segment of the type IIA Na channel α subunit that are important for the action of local anesthetics on either resting, or open and inactivated channels. We have now examined effects of these mutations on block by the antiarrhythmics lidocaine and quinidine and by the anticonvulsant phenytoin. The mutant N1769A increased block of resting channels by phenytoin and lidocaine 2-3 fold compared to wild type. In contrast, mutations F1764A and Y1771A almost completely abolished the voltage- and frequency dependence of block by phenytoin, lidocaine and quinidine, indicating that these mutations caused large decreases in the affinity of open and inactivated channels for drugs. Mutation I1760A accelerated drug escape from closed channels, without altering channel affinity. Based on these results, we propose that local anesthetics, anticonvulsants and antiarrhythmics bind to residues F1764 and Y1771, whereas I1760 controls access to this receptor site and N1769 modulates affinity of the site by an allosteric mechanism.

**W-AM-H4**

COORDINATION OF $Ca^{2+}$ BY THE PORE REGION GLUTAMATES IS ESSENTIAL FOR HIGH AFFINITY DIHYDROPYRIDINE (DHP) BINDING TO CARDIAC $Ca^{2+}$ CHANNEL $\alpha_1$-SUBUNIT. ((J. Mitterdorfer, M.J. Sinnegger, M. Grabner, M. Froschmayr, J. Striessnig and H. Glossmann)) Institut für Biochemische Pharmakologie, Universität Innsbruck, Peter Mayrstr.1, A-6020 Innsbruck, Austria

A $Ca^{2+}$ channel $\alpha_1$-subunit derived from rabbit heart was transiently expressed in COS-7 cells. The dihydropyridine (+)-isradipine had low affinity ($K_i$ = 34.3 nM; $k_{-1}$ = 0.11 $min^{-1}$) for the $\alpha_1$-subunit in the absence of the ß-subunit. Co-expression of the ß-subunit resulted in an >35-fold increase in (+)-isradipine binding affinity ($K_i$ = 0.9 nM; $k_{-1}$ = 0.007 $min^{-1}$), which was associated with an increase of the apparent affinity of $Ca^{2+}$ ions for the channel as revealed by the decrease of the $Ca^{2+}$ dissociation rate ($k_{-1}$ = 2.16 $min^{-1}$ for $\alpha_1$; $k_{-1}$(I) = 0.73 $min^{-1}$ (27 %) and $k_{-1}$(II) = 0.014 $min^{-1}$ (73 %) for $\alpha_1$ß). To investigate the role of the P-region glutamates in the $Ca^{2+}$ dependence of high affinity DHP binding a series of single mutants (E393Q, E736Q, E1145Q and E1446Q) and a double mutant (E393Q+E736Q) were generated and co-expressed with the ß-subunit. (+)-[$^3$H]isradipine binding activity was almost completely abolished in all mutants and could be partially recovered by the allosteric modulator (+)-tetrandrine in mutants E393Q and E736Q, but not in mutants E1145Q, E1446Q and the double mutant. Our results suggest that high affinity DHP binding is dependent on the ß-subunit-induced conformational stabilization of the glutamate residues which form the $Ca^{2+}$ coordination site of the channel pore. (Supported by FWF grants S6601-med (H.G.), S6602-med (J.S.) and Dr. Legerlotz-Stiftung (H.G.,M.G.,J.M.)

**W-AM-H5**

GLUTAMATE 363 OF THE CYCLIC GMP-GATED CHANNEL CONTROLS BOTH THE SINGLE CONDUCTANCE AND THE OPEN PROBABILITY ((F. Sesti*, U.B. Kaupp+, E. Eismann+, M. Nizzari* and V. Torre*)) *Dipartimento di Fisica, Via Dodecaneso 33, Genova, Italy and +Institut fur Biologische Informationsverarbeitung, D-52425 Jülich, Germany

The cGMP-gated channel cloned from bovine rods has a single-channel conductance of about 27 pS and in the presence of a saturating cGMP concentration of 500μM the open probability is 0.75 ± 0.04 at -100 mV and 0.76 ± 0.05 at +100 mV. When glutamate was substituted with aspartate the single-channel conductance increased to 32 pS at +100 mV and to 48 pS at -100 mV and a subconducting state of 30 pS could be observed at negative membrane voltages. The open probability of the mutant E363D in the presence of saturating cGMP concentrations was 0.85 ± 0.05 at +100 mV and 0.67 ± 0.04 at -100 mV. No single-channel events could be detected in mutants E363Q and E363A, and noise analysis indicates that the single-channel conductance was reduced to about 1-2 pS. The single-channel conductance of the mutant E363N was about 14 pS both at +100 and -100 mV, and the open probability in the presence of saturating cGMP concentrations was highly voltage dependent and was 0.4 ± 0.1 at +100 mV and 0.06 ± 0.03 at -100 mV. These results indicate that glutamate 363 besides controlling the single-channel conductance, plays a fundamental role in determining the gating of the channel and the voltage dependence of its open probability.

**W-AM-H6**

STRUCTURAL MODEL OF ION SELECTIVE REGIONS OF EPITHELIAL SODIUM CHANNELS. ((H. Robert Guy and Stewart R. Durell)) Lab. of Math. Biology, DCBDC, NCI, NIH, Bethesda, MD 20892.

Epithelial sodium channels are comprised of homologous α, β, and γ subunits (Canessa *et al.* 1994 Nature 367:463-467). Each subunit has two hydrophobic segments, M1 and M2, that probably form transmembrane α helices. M1 and M2 are preceded by segments that are highly conserved among the subunits and in putative mechanosensitive channels from *C. Elegans*. We postulate that these segments from 3α, 3β, and 3γ subunits form ion selective αβ barrel structures; the inner pre-M1 αβ barrel extends into the cytoplasmic entrance of the pore and the outer pre-M2 αβ barrel is at the extracellular entrance of the pore. Projections showing residues lining the interior of these barrels are shown below. The backbones of the putative core β barrels have 3-fold radial symmetry with homologous residues of adjacent strands staggered along the pore. In the outer barrel glutamines form the narrowest and probably most ion selective region, glycines allow tryptophan side chains to pack against the α barrel's wall, and serines bind to the tryptophans.

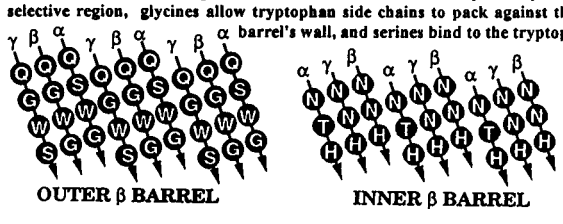


OUTER β BARREL INNER β BARREL

**W-AM-H7**

MAPPING THE SODIUM CHANNEL PORE: SINGLE CYSTEINES IN EACH OF THE P LOOPS CONFER SENSITIVITY TO BLOCK BY $Cd^{2+}$. ((M. Teresa Perez-Garcia, Nipavan Chiamvimonvat, Eduardo Marban, Gordon F. Tomaselli)) Dept. of Medicine, Johns Hopkins University, Baltimore MD

The only naturally variant cysteine (cys) within the P loops of Na channels occurs in domain I of the cardiac isoform, where it confers sensitivity to block by external $Cd^{2+}$ and resistance to TTX. Mutation of the divergent tyrosine in the $Cd^{2+}$-resistant ($K_d$ = 1.7 mM) μ1 isoform to cysteine (Y401C) renders the mutant $Cd^{2+}$-sensitive ($K_d$ = 17 μM). Single-channel Woodhull analysis of the $Cd^{2+}$ block reveals a fractional electrical distance (δ) of 20-25% from the outside. Likewise, cys conversion of the neighboring residue (W402C) increases $Cd^{2+}$ blocking affinity ($K_d$ = 133 μM), with δ ~ 18%. To determine which residues line the pore and their relative positions within the transmembrane electrical field, we substituted with cys individual residues at the 401- and 402-equivalent positions in domains II-IV, identified by sequence alignment. At the positions corresponding to residue 401, the domain II and IV mutants (W756C & G1530C) both exhibit a measurable but small increase in $Cd^{2+}$ blocking affinity compared with the wild type μ1 ($K_d$ = 860 & 1040 μM, respectively). Interestingly, the domain II and III cys substitutions at the 402-equivalent position are much more $Cd^{2+}$-sensitive (I757C: 152 μM; W1239C: 101 μM). W1239C exhibits flicker block by $Cd^{2+}$ with δ ~ 19%. The results available to date suggest a high degree of symmetry at the 402-analogous position, but marked differences among domains at the preceding residue.

**W-AM-H8**

CYSTEINE CONVERSION OF ACIDIC RESIDUES IN THE OUTER MOUTH RENDERS Na CHANNELS SENSITIVE TO BLOCK BY $Cd^{2+}$ ((Nipavan Chiamvimonvat, M. Teresa Pérez-García, Kimberly Kluge, Gordon F. Tomaselli, Eduardo Marban)) Dept. of Medicine, Johns Hopkins University, Baltimore MD 21205.

Among mammalian Na channel isoforms, those sensitive to TTX are resistant to block by external $Cd^{2+}$, and vice versa. The external ring of negative charges in the P loops of Na channels is known to influence TTX binding (Terlau *et al*, *FEBS Lett* 293:93-6, 1991). In the $Cd^{2+}$- resistant ($K_d$,Cd = 1.7 mM), TTX-sensitive ($K_d$,TTX = 17 nM) μ1 isoform, we mutated individual residues to cysteine to probe the relationship between TTX and $Cd^{2+}$ block affinities. Deeper in the P loops, single cysteine conversions suffice to confer high-affinity $Cd^{2+}$ block (Pérez-García *et al.*, this meeting), while generally rendering the channels less TTX-sensitive. Conversion of each of the external charged residues in domains II-IV to cysteine renders the mutants $Cd^{2+}$-sensitive while having variable effects on TTX sensitivity (see table). The domain II and IV mutants E758C and D1532C both exhibited enhanced $Cd^{2+}$ blocking affinity and diminished TTX sensitivity. In contrast, the domain III mutant D1241C was very sensitive to block by both $Cd^{2+}$ and TTX. Thus, sensitivities to $Cd^{2+}$ and to TTX are not always reciprocally related.

| | $K_d$,Cd (μM) | $K_d$,TTX (nM) |
|---|---|---|
| WT | 1700 | 17 |
| E758C | 320 | >100000 |
| D1241C | 147 | 2 |
| D1532C | 193 | 1030 |

## MOLECULAR RECOGNITION AND BINDING III

**W-AM-I1**

ON A MECHANISM FOR DRUG RESISTANCE IN THE HIV-1 PROTEASE. ((F. Sussman, M. C. Villaverde and V. Nauchitel)) Protein Studies Section, Oklahoma Medical Research Foundation. Oklahoma City, O.K. 73104,

One of the biggest hurdles to overcome in the development of anti-viral drugs directed towards the HIV-1 protease (HIV-1 PR) is the formation of drug-resistant virions through the generation of resistance mutations in the target protein. To understand the way a mutated HIV-1 PR enzyme lowers its affinity for some inhibitors we have modeled the energetics of inhibitor binding to 'resistance' mutants using as a starting point a series of mutational experiments at position 82 of this enzyme. In all cases it has been observed that the largest reduction in binding is provided by the Val-82 to Asp or Val-82 to Asn mutations. The Val-82 to Glu or to Gln are less deleterious to the inhibitor binding constants. Our calculations demonstrate that the actual binding does not result directly from the stability of the bound state and that the reference unbound state plays a crucial role in the reduction of binding affinity for the HIV-1 PR inhibitors upon mutation. Theses results have lead us to postulate some plausible strategies for the design of inhibitors that are inmune to resistant mutations.

This work was supported by N.I.H. and O.C.A.S.T. grants.

**W-AM-I2**

FLUOROGENIC SUBSTRATES FOR THE DETECTION OF PROTEASES. ((Beverly Z. Packard, Akira Komoriya, and Ludwig Brand)) Oncolmmunin, Inc., P.O. Box 2155, Kensington, MD 20891 and Biology Department, Johns Hopkins University, Baltimore, MD 21218

Proteases are involved in normal tissue functions as well as in certain pathologic processes; therefore, it is important to have assays to detect their presence and activities. One can design new synthetic substrates by following the structure of their natural substrates, *i.e.*, protease inhibitors. Thus, the synthesis of amino acid sequences or mimetics thereof found at the active sites of protease inhibitors, followed by covalent attachment of fluorescent probes on the peptide termini, can be used to characterize activities of proteases. We now describe the synthesis of a modified peptide sequence from the serpin $\alpha_1$-antitrypsin and the derivatization of its termini with two different sets of fluorophores. The choice for both sets was based on the emission of one member overlapping with the excitation of the other. Upon cleavage of the doubly-labeled peptides by elastase, a protease with specificity for $\alpha_1$-antitrypsin, a three- to ten-fold enhancement of fluorescence can be observed. The influence of cleavage upon the fluorescence of both singly- and doubly-labeled peptides will be described.

**W-AM-I3**

DEVELOPMENT OF RAPID SCREENING ASSAYS FOR A NEW CLASS OF ANTIVIRAL DRUGS ATTACKING ZINC FINGERS IN RETROVIRAL NUCLEOCAPSID PROTEINS ((J. R. Casas-Finet, C. A. Schaeffer, R. C. Sowder II, L. E. Henderson, L. O. Arthur, and W. G. Rice)) PRI/DynCorp, NCI-FCRDC, Frederick, MD 21702. (Spon. by J. W. Erickson)

All nucleocapsid (NC) proteins of the Oncovirinae and Lentivirinae subfamilies of Retroviridae contain sequences of 14 amino acids with 4 invariant residues, $C(X)_2C(X)_4H(X)_4C$, which chelate zinc through His imidazole and Cys thiolates. These structures are referred to as retroviral CCHC Zn fingers and are one of the most highly conserved features of the Retroviridae family. HIV-1 NC protein contains two Zn fingers 7 amino acids apart; mutational analysis has shown that both are required during viral assembly for packaging genomic RNA and, in addition, are essential for early events in the virus infection process. We previously suggested that retroviral CCHC Zn fingers are ideal targets for rational drug design because of their extreme conservation among Retroviridae and their essential roles in two separate steps of viral replication. C-nitroso compounds inactivate HIV-1 by attacking the CCHC Zn fingers and ejecting Zn(II) from the virus [Rice *et al., Nature 361*, 473-475 (1994)]. A study of the mechanism of the reaction revealed that CCHC Zn finger coordination complexes act as electron donors to suitable Lewis bases. The reaction displaces Zn(II), converts the conserved thiolates to disulfides and destroys the active conformation of retroviral CCHC Zn fingers. Numerous electrophilic reagents function as electron acceptors for the reaction with HIV-1 NC protein. High-throughput fluorimetric assays have been developed to allow fast screening of compounds for activity against retroviral Zn fingers. The fluorescence emission intensity of a $(dT)_8$ oligonucleotide fluoresceinated at both ends increases upon binding of HIV-1 NC protein (p7), and treatment of p7/oligonucleotide complexes with certain thiolate-reactive compounds results in their disruption and concomitant decrease of fluorescence signal. Destruction of the metal binding site in p7 can be monitored with fluorescent metal-chelating probes. Activity against NC proteins of HIV-1 (or the non-human pathogenic EIAV or BLV) in the intact viruses can be assessed by analysis of their SDS-PAGE migration pattern. Using this target-based screen, the NCI Drug Discovery Program has identified and developed compounds that belong to a new class of drugs attacking highly conserved Zn finger structures in HIV and related retroviral NC proteins.

**W-AM-I4**

INTERACTION OF FATTY ACIDS WITH NATIVE AND MUTANT FABPS MONITORED WITH ADIFAB. "Gary V. Richieri, Ronald T. Ogata, and Alan M. Kleinfeld" Medical Biology Institute, La Jolla CA.

The interactions of long chain fatty acids (FA) with native and mutant fatty acid binding proteins (FABPs) have been measured by using the fluorescent probe ADIFAB, the acrylodan labeled intestinal FABP, to monitor the unbound or free fatty acids (FFA). ADIFAB allows one to measure the interactions of FA with the unlabeled proteins without physical separation of any of the reactants. Application of this method (Richieri et al, J. Biol. Chem., 1994 269:23918) to the equilibrium binding of palmitate, stearate, oleate, linoleate, linolenate, and arachidonate to FABPs from adipose, intestine, heart, and liver reveals that, in contrast to previous studies, dissociation constants ($K_d$) are extremely sensitive to the tissue origin of the FABP and the molecular species of FA. For example, the order of $K_d$s for oleate is, adipose>intestine>liver>heart. $K_d$ values for fatty acids with the same chain length were considerably lower for saturated as compared to polyunsaturated FA, consistent with the lower aqueous solubilities of the saturated fatty acids. The measured $K_d$s at 37°C which ranged from about 2 to 1000 nM, depending upon the tissue origin of the FABP and the FA, are generally more than 100 fold smaller than obtained by other methods. Crystallography results suggest that fatty acids can enter the FABP binding site through a specific portal region. Site-specific mutations in this (portal) region of the adipocyte and intestine proteins exhibit alterations in the FA binding characteristics that are consistent with the portal hypothesis. Mutations involving amino acids that are involved in the interaction with the FA carboxyl group, yield binding properties that do not exhibit a simple correlation with predictions based upon the crystal structure. This work was supported with grant GM46931 from the NIH.

**W-AM-I5**

**SYNTHESIS OF A FLUORESCENT THAPSIGARGIN DERIVATIVE AND DEMONSTRATION OF ITS INHIBITORY INTERACTION WITH A Ca2+ MEMBRANE BOUND DOMAIN.** ((S. Hua, H. Malak, J. R. Lakowicz and G. Inesi)) Department of Biological Chemistry, Center for Fluorescence Spectroscopy and Medical Biotechnology Institute, School of Medicine, University of Maryland, Baltimore, MD 21201. (Spon. by K. Collins)

A fluorescent derivative (DTG) of thapsigargin (TG) was synthesized by replacing the C8-butanoyl chain with a dansyl moiety. Its structure was confirmed by NMR spectroscopy. Functional studies indicated that DTG retains the inhibitory effect of TG on the sarcoplasmic reticulum (SR) ATPase, displaying a 2 $\mu$M $K_I$. Steady state fluorescence measurements were consistent with energy transfer to DTG from tryptophanyl residues assigned to the ATPase membrane bound region. This phenomenon exhibited saturation behavior, occurred in the presence of DTG concentrations producing ATPase inhibition, and was prevented by inhibitory concentrations of TG. No energy transfer between DTG and a fluorescein 5'-isothiocyanate (FITC) label of the ATPase extramembranous region was detected. These observations suggest the inhibitory TG binding domain resides within or near the membrane bound region of the ATPase. (Supported by NIH grants to J.R.L. and G.I.)

**W-AM-I6**

***In -Situ* Microscopy of Two-Dimensional Streptavidin Crystallization** ((W. Frey, W. R. Schief, A. Chilkoti, P. S. Stayton, V. Vogel)) Center for Bioengineering, University of Washington, Seattle, Wa. 98195, USA.

We introduce Brewster angle microscopy (BAM) for the study of two-dimensional protein aggregation and crystallization underneath lipid monolayers at the air-water interface. This technique is sensitive to the surface layer only and is able to resolve the lateral protein density distribution without the need of a label. Here we simultaneously combine BAM and fluorescence microscopy to observe the formation of crystalline domains of commercial "full-length"- streptavidin and recombinant "core"-streptavidin bound to a biotinylated lipid monolayer.

Simultaneous observation with BAM and fluorescence microscopy shows that the crystals, typical for labeled "full-length" streptavidin are congruent and are of the same shape and size as for the unlabeled protein. Recombinant "core"-streptavidin, which lacks flexible loops and lysine residues easily accessible for label attachment, forms domains of larger size and different shape compared to commercial streptavidin. Label attachment is possible and does not affect the crystal shape only if the labeling ratio is low. Combination of both methods reveals a structural reorganization of the crystals in the first 20 minutes after protein injection. Insight into the crystal formation process is delineated from these observations.

**W-AM-I7**

MEASUREMENTS OF THE INTERFACIAL FREE ENERGY OF FUNCTIONALIZED SURFACES USING REFLECTION INTERFERENCE CONTRAST MICROSCOPY ((H. Lehmann, V.T. Moy, T.J. Feder, M. Rief, H.E. Gaub and E.Sackmann)) Biophysics Group, Department of Physics, Technische Universität München, 85747 Garching, Germany. (Spon. by T.J. Feder)

The deformation of functionalized agarose beads resulting from their interaction with an opposing functionalized substrate provide a means to measure the interaction energy between surfaces. The interfacial free energy of interacting elastic spheres can be calculated from the focal contact area using the JKR/Hertz model. Reflection interference contrast microscopy was used to measure the focal contact area between beads and substrate. Adopting this technique, we have measured the interfacial energy for different combinations of modified surfaces in solution, including the specific interaction of surfaces functionalized with ligands and receptors. The interfacial free energy shows dependence on pH, electrolyte concentration, and the chemistry of the electrolyte.

**W-AM-I8**

**EFFECTS OF NEUTRAL SOLUTES AND OSMOTIC PRESSURE ON THE ACTIVITY OF ASPARTATE TRANSCARBAMYLASE** ((Vince J. LiCata, Jaishree Trikha, and Norma M. Allewell)) Department of Biochemistry, University of Minnesota, St. Paul, MN 55108

*E. coli* aspartate transcarbamylase (ATCase) catalyses the first committed step in pyrimidine biosynthesis: the condensation of aspartate and carbamyl phosphate to produce carbamyl aspartic acid and inorganic phosphate. In the presence of saturating amounts of carbamyl phosphate, ATCase binds aspartate cooperatively, and is allosterically activated by ATP and inhibited by CTP.

In order to assess the relationship between heterotropic regulation of the enzyme and tertiary conformational changes that might be reflected in differential water binding, we have begun to examine ATCase activity and nucleotide regulation in the presence of various osmolytes. PEG-8000, PEG-300, sucrose, and dextran-11,000 all alter both the Km and Vmax values for aspartate. Solute effects on Km vary in a solute size dependent manner: the two smaller molecules increase substrate affinity similarly and yield a calculated release of ~50 waters upon binding of aspartate, while the two larger solutes decrease substrate affinity and yield a calculated binding of ~100 waters. Calculated relative changes in water binding indicate that the technique will detect differential solvation upon binding of regulatory nucleotides. All four osmolytes decrease Vmax in a fashion that is most dependent on the weight percent of polymer, or the viscosity of solution. Calculations of the solvent accessible surface area of ATCase in the presence and absence of substrates and nucleotide effectors and their dependence on probe size will also be presented. Supported by NIH Grant DK-17335 (N.M.A.) and NIH Fellowship GM-14400 (V.J.L.).

**W-AM-I9**

**OLIGOMERIC STRUCTURE OF THE CLP-AP PROTEASE FROM E.coli.** ((M. Kessel*+, B. Kim*, B.L. Trus*#, E. Kocsis*, S.K. Singh**, M. Maurizi**and A.C. Steven*)) LSBR-NIAMS*, LCB-NCI**, CSL-DCRT#, NIH, Bethesda MD 20892 and the Hebrew University-Hadassah Medical School, Jerusalem, Israel+. (Spon. by L. M. Amende)

Intracellular protein degradation is >90% energy-dependent, arousing much interest in the specificity and mechanism of action of ATP-dependent proteases. The ClpAP enzyme is composed of two proteins - ATP-hydrolyzing ClpA and proteolytic ClpP - which interact in the presence of ATP to form an active protease. ClpP has a subunit $M_r$ of 21,500 and forms an oligomer of $M_r$ ~250,000 as estimated by analytical ultracentrifugation, indicating about 12 subunits. When examined by EM after negative staining with 1% uranyl acetate, ClpP appears as an 11nm diameter donut-shaped particle. Image analysis of four independent data sets with a novel symmetry detection algorithm consistently revealed seven-fold rotational symmetry, indicating that ClpP is a double ring of 2x7 subunits. ClpA (subunit $M_r$ ~83,000) forms an oligomer of ~ 500,000 and has two distinct ATP binding sites per subunit. EM shows ClpA as morphologically heterogeneous particles of which a subset shows two parallel striations, corresponding to a side view of a single ring of bilobed subunits. Image analysis detected a small subset with sixfold rotational symmetry. ClpAP complexes have $M_r$'s of either 800,000 or >1 million depending upon whether one or two ClpA oligomers interact with a single ClpP oligomer. By EM, the 1:1 complex of ClpA and ClpP appears in side view with both oligomeric rings stacked axially to form a barrel-like particle. The 2:1 complex has an additional ClpA bound to the opposite face of ClpP. Assuming that ClpA is indeed sixfold symmetric, these observations imply a symmetry mismatch in the axial stacking of ClpA and ClpP to form active complexes.

W-AM-J1

ELECTROSTATIC EFFECTS AND PROTON CONDUCTION IN BACTERIAL REACTION CENTER PROTEIN ((D. K. Hanson and M. Schiffer)) Argonne Natl. Lab., 60439, IL., USA. ((J. D. Delcroix and P. Sebban)) C.G.M., CNRS, 91198, Gif, France.

Light-induced charge separation in the photosynthetic reaction center results in delivery of two electrons and two protons to the quinone terminal acceptor, $Q_B$. In *Rhodobacter capsulatus*, we have previously shown that this function is strongly impaired in a photosynthetically incompetent reaction center mutant, $Glu^{L212}/Asp^{L213}$ → $Ala^{L212}/Ala^{L213}$ (P. Maroti, D.K. Hanson, L. Baciou, M. Schiffer and P. Sebban (1994) *Proc. Natl. Acad. Sci.* 91, 5617-5621). The function recovery of two photo-competent derivatives that carry both alanine substitutions and an intergenic suppressor mutation located far from $Q_B$ (Ala-Ala + $Arg^{L217}$ → Cys (∿ 11 Å); Ala-Ala + $Asn^{M5}$ → Asp (∿ 15 Å) has been studied by flash-induced absorbance spectroscopy. The electrostatic influence of the protein in proton conduction and delivery to $Q_B$ is suggested.

W-AM-J2

ENDOR STUDIES OF $Q_A^-$ IN SINGLE CRYSTALS OF REACTION CENTERS FROM *Rb. SPHAEROIDES*.* ((R.A. Isaacson, E. Abresch, G. Feher)) Phys. Dept., Univ. of Calif., San Diego, La Jolla, CA 92093. ((W. Lubitz)) Max-Volmer Institut, Techn. Univ. Berlin, D-10623, Berlin, Germany. ((J.C. Williams and J.P. Allen)) Chem. Dept., Arizona State Univ., Tempe, AZ.

For ENDOR studies of the primary acceptor $Q_A^-$, the magnetically interacting $Fe^{2+}$ in native bacteria must be replaced by diamagnetic $Zn^{2+}$ (1). The replacement was accomplished by biosynthetic growth in low Fe/high Zn media of i) native bacteria or ii) mutants His M266 → Cys. Method i) produces 20-30% Zn replacement compared to >90% for method ii). $Q_A^-$ was generated by dithionite reduction under Argon. The ENDOR spectra of the two preparations were similar. From the ENDOR results on single crystals, the angular variation of the hyperfine couplings (hfc) of three types of protons was obtained (see Fig.); i.e. of the methyls ($CH_3$), the methylenes ($CH_2$) and the exchangeables (xxx). The exchangeables are assigned to H-bonds between the quinone oxygens and protein residues. (1) Feher, Isaacson, Okamura & Lubitz (1985) *Springer Series, Chem. Phys.* 42, p. 174. *Work supported by NIH, NSF, DFG and NATO.

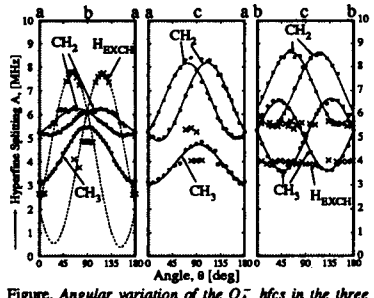


Figure. *Angular variation of the $Q_A^-$ hfcs in the three crystallographic planes of Zn RC single crystals of the HC (M266) mutant, $\nu_e \cong 9$ GHz, T=3°C.*

W-AM-J3

THE ROLE OF HYDROGEN BONDED PROTONS IN THE PHOTOCHEMICAL REDUCTION OF $Q_B$ TO $Q_BH_2$ IN REACTION CENTERS OF *RB. SPHAEROIDES*.*
((M.L. Paddock, E. Abresch, R.A. Isaacson, G. Feher & M.Y. Okamura)) Phys. Dept., Univ. of Calif. San Diego, La Jolla, CA 92093.

In bacterial reaction centers (RCs) two protons participate in hydrogen bonds to the carbonyl oxygens of $Q_B$. We used ENDOR spectroscopy to determine whether these protons are transferred to photochemically reduced $Q_B$. The two H-bonded protons gave rise to two ENDOR lines (labeled "a" & "b" in the Figure) [1]. To eliminate interference from the high spin $Fe^{2+}$, RCs containing $Zn^{2+}$ were isolated from a His-M266 → Cys mutant, which more easily incorporate $Zn^{2+}$ (see abstract by Isaacson *et al*). From the ENDOR amplitude the exchange rates of H with D in RCs diluted into $D_2O$ were determined to be << 10s for proton "a" and ~20s for proton "b". Proton "a" is tentatively assigned to Ser-L223 and proton "b" to the solvent inaccessible His-L190 [2]. By using multiple laser flashes the H exchange rate of proton "b" should increase to the rate of $Q_BH_2$ formation if the "b" proton is used in the formation of $Q_BH_2$. This was not found to be the case implying that the "b" proton remains in the RC. Hence the "b" proton is not part of a proton transfer chain. [1] Feher, G., Isaacson, R.A., Okamura, M.Y. & Lubitz, W. (1985) *Springer Chem. Phys. Ser.* 42, p. 174. [2] Allen, J.P., Feher, G., Yeates, T.O., Komiya, H. & Rees, D.C. (1988) *Proc. Natl. Acad. Sci. USA* 85, 8487. *Work supported by NIH & NSF.

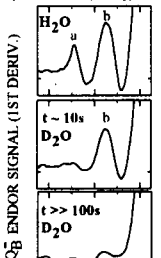


*Low frequency side of $Q_B^-$ ENDOR spectra ($\nu$=9GHz, T=-30C).*

W-AM-J4

SUGGESTED ROLE OF AN INTERNAL WATER MOLECULE IN PROTON TRANSFER IN A SER-L223 → GLY SITE-DIRECTED MUTANT REACTION CENTER FROM *RB. SPHAEROIDES*.*
((M. L. Paddock, G. Feher & M. Y. Okamura)) Dept. of Physics 0319, 9500 Gilman Dr., University of California San Diego, La Jolla, CA 92093-0319.

The bacterial reaction center (RC) converts light into chemical energy through the double reduction and protonation of a bound quinone molecule $Q_B$. A drastic reduction ($10^2$ at pH 7.5) in $k_{AB}^{(2)}$ ($Q_A^-Q_B + H^+ \rightarrow Q_AQ_BH^-$) measured in RCs where Ser-L223 was replaced with Ala (1) suggested that Ser-L223 plays a critical role in proton transfer to reduced $Q_B$. In contrast, replacement of Ser-L223 with Gly was found to retain fast proton transfer rates (see Figure). Similarly other electron transfer rates involving $Q_B$ were not significantly affected by the Gly replacement suggesting that the structure near $Q_B$ is unaltered in the mutant RCs. This suggestion is further supported by analysis of the crystal structure of the Ser-L223 → Gly RCs in which no major changes in the backbone structure are seen compared to native RCs (see following abstract by Axelrod *et al.*). It is proposed that in the Ser-L223 → Gly mutant RCs, a water molecule functions in place of the missing hydroxyl group of the L223 residue. (1) Paddock, M. L., McPherson, P. H., Feher, G. & Okamura, M. Y. (1990) *Proc. Natl. Acad. Sci. USA* 87, 6803. *Supported by NIH and NSF.

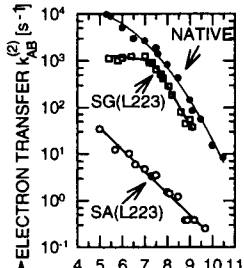


*Figure. Proton-coupled electron transfer rate $k_{AB}^{(2)}$ for native, SA(L223) [Ser-L223 → Ala] and SG(L223) [Ser-L223 → Gly] as a function of pH.*

W-AM-J5

AN INTERNAL $H_2O$ CHAIN IN CYTOCHROME *f*. ((S. E. Martinez, W. A. Cramer and J. L. Smith)) Department of Biological Sciences, Purdue University, West Lafayette IN 47907

Refinement of the atomic model for the 252-residue lumen-side domain of cytochrome *f* at a resolution of 1.96 Å revealed the presence of five internal water molecules, four of which define a vector-like pathway that extends 12 Å from the His25 heme ligand to a solvent-accessible space within 6 Å of Lys66. Lys66 is part of a basic domain also containing Lys65, Lys58, and possibly Lys187, which has been proposed to form a docking site for carboxylate residues of the acidic electron acceptor, plastocyanin. Residues Asn232, Gln59, and Asn168, which are in a position (ca. 3 Å, respectively from each O atom) to form H-bonds with the last three $H_2O$ in the chain, are identical in 13 cyt *f* sequences. Asn153, which can H-bond to the $H_2O$ that is H-bonded to His25, is conserved in 12 of 13, the exception being *V. fabia*, where it is Thr. Gln158, which can form an H-bond with a fifth water that is not in the linear chain, is conserved in all 13 sequences. The five waters also make a total of six H bonds to backbone carbonyls and amides. The existence of the vectorial $H_2O$ chain in cyt *f* suggests: (a) cyt *f* functions in the pathway of $H^+$ extrusion from the cytochrome $b_6f$ complex; (b) the water chain in cyt *f* proximal to His25 functions as the terminal link in an inter- and intraprotein $H^+$ translocation pathway that starts with the oxidation of plastoquinol; (c) this last link in the $H^+$ transfer pathway could utilize carboxylate residues of the bound electron acceptor, plastocyanin, as the terminal $H^+$ acceptor; (d) protonation of PC carboxylates could also provide the reaction needed to release reduced PC from cyt *f*. Consistent with a role of cyt *f* in the pathway of $H^+$ extrusion, the $E_m$ of cyt *f* is pH-dependent with a pK *in vitro* for the oxidized state of approximately 8.0-8.5 (Davenport and Hill, 1952; Ponomarev, Everly and Cramer, unpubl. data). (Supported by USDA 9301586; NIH GM-38323)

W-AM-J6

THE MECHANISM OF PROTON-COUPLED ELECTRON TRANSFER TO $Q_B$ IN REACTION CENTERS FROM *RB. SPHAEROIDES*.*
((M.S. Graige[1], M.L. Paddock[1], A. Labahn[1], J.M. Bruce[2], G. Feher[1], M.Y. Okamura[1])) [1]Dept. of Physics, University of California San Diego, 9500 Gilman Dr., La Jolla, CA 92093-0319. [2]Dept. of Chemistry, University of Manchester, Manchester M139PL, U.K.

Reduction of the secondary quinone, $Q_B$, in bacterial reaction centers (RCs) involves the sequential transfer of two electrons from the primary quinone, $Q_A$. The second electron transfer step, $k_{AB}^{(2)}$ ($Q_A^-Q_B^- + H^+ \rightarrow Q_AQ_BH^-$), is coupled to proton uptake and can be modeled as one of four possible consecutive two-step mechanisms. Case 1: proton transfer preceding rate limiting electron transfer. Case 2: rate limiting proton transfer preceding electron transfer. Case 3: electron transfer preceding rate limiting proton transfer. Case 4: rate limiting electron transfer preceding proton transfer. To test these mechanisms, $k_{AB}^{(2)}$ was measured in RCs with lower potential quinones (1,2) in the $Q_A$ site and ubiquinone ($Q_{10}$) in the $Q_B$ site (see abstract by Labahn *et al.*). These substitutions should increase the electron transfer rate between $Q_A$ and $Q_B$ without affecting the proton transfer rate. Predicted behavior of $k_{AB}^{(2)}$ for the four cases is depicted in the figure. The data are consistent with the predictions of cases 1 and 4 and exclude cases 2 and 3. An argument has been presented against case 4 (3). Consequently, we propose case 1 as the dominant mechanism for $k_{AB}^{(2)}$. However, a mechanism involving simultaneous transfer of both an electron and a proton can not at present be ruled out. (1) Woodbury *et al.*(1986), Biochim.Biophys. Acta., 851, 6. (2) Gunner *et al* (1989), J. Am. Chem. Soc., 111, 3400. (3) Paddock *et al.*(1994), Biochem., 33, 734. *Supported by NIH, NSF, NATO/DAAD & Deutsche Forschungsgemeinschaft.

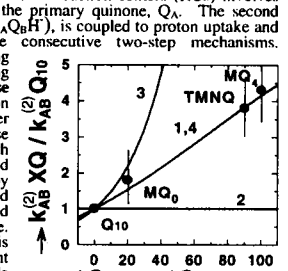


*Normalized $k_{AB}^{(2)}$ rate vs. change in free energy of various quinones with respect to native $Q_A$. Numbered curves represent the predicted dependencies of the 4 cases. $Q_{10}$= Ubiquinone-10, MQ = Menaquinone, TMNQ = 2,3,5-trimethyl-1,4-naphthoquinone, XQ= MQ or TMNQ. pH=7.2, T=23° C.*

W-AM-J7

## X-RAY CRYSTALLOGRAPHIC ANALYSIS OF A SITE-DIRECTED PROTON TRANSFER MUTANT SER-L223→GLY OF THE BACTERIAL RC FROM *RB. SPHAEROIDES*.

(( H.L. Axelrod, E. Abresch, M.L. Paddock, M.Y.Okamura, and G. Feher)) Dept. of Physics, Univ. of Calif. San Diego, La Jolla, CA 92093-0319. ((D.C. Rees)) Division of Chemistry and Chemical Engineering 147-75CH, Calif. Institute of Technology, Pasadena, CA 91125.

In reaction centers (RC) of *Rhodobacter sphaeroides*, light induces the transfer of two electrons and two protons to a bound quinone acceptor, $Q_B$. The hydroxyl sidechain of Ser-L223 near $Q_B$ in the native structure (see figure) is involved in the transfer of protons to reduced $Q_B$ in native RC's (1). In the site-directed mutant, SG(L223) (Ser-L223→Gly), an alternate proton donor replaces the serine hydroxyl as shown by the first proton-coupled electron transfer rate, $k_{AB}^{(2)}$, in SG(L223) RC's (see previous abstract by Paddock *et. al.*). To gain structural information on this mutant, SG(L223) RC's were crystallized in the same form as wild type RC's (2), and x-ray diffraction intensities were measured to a resolution of ~3.5 Å. Difference electron density maps, wild type minus SG(L223), show the absence of serine sidechain density in the mutant (see dotted lines in the figure), and do not indicate significant rearrangement of protein in this region. Assuming the wild type positioning of $Q_B$, the lack of structure change in the mutant suggests that, most likely, a water molecule replaces the serine sidechain as the proton donor. (1) M.L. Paddock, P.H. McPherson, G. Feher, and M.Y. Okamura *PNAS* **87**, 6803-6807 (1990). (2) J.P. Allen and G. Feher *PNAS* **81**, 4795-4799 (1984). *Work supported by NIH and USDA.

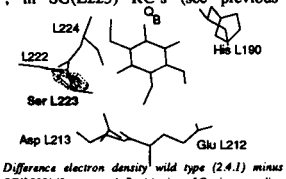


*Difference electron density wild type (2.4.1) minus SG(L223) (3σ contour). Positioning of $Q_B$ is according to native structure.*

W-AM-J8

## IMPORTANCE OF A CARBOXYLIC ACID AT H173 FOR PROTON-COUPLED ELECTRON TRANSFER IN RCs OF *RB. SPHAEROIDES**.

((S. H. Rongey, A. L. Juth, M. L. Paddock, G. Feher & M. Y. Okamura)) Physics Dept. 0319, 9500 Gilman Dr., UC San Diego, La Jolla, CA 92093.

The reaction center (RC) uses light to reduce and protonate $Q_B$, a bound quinone. This process involves the proton-coupled electron transfer reaction: $Q_A Q_B^- + H^+ \rightarrow Q_A Q_B H^-$ ($k_{AB}^{(2)}$). The protons involved in this process are transferred by a chain of protonatable amino acid residues including Asp-L213 (1,2). To determine whether Glu-H173, which is close to Asp-L213 and solvent accessible, is important for proton transfer it was replaced with Gln and Asp. Replacement of Glu-H173 with Gln decreases $k_{AB}^{(2)}$ ~10 fold, while a change to Asp does not effect $k_{AB}^{(2)}$ (see Fig.). These results indicate an acid residue at H173 is important for rapid proton-coupled electron transfer to $Q_B^-$, either to act as a proton donor, presumably to Asp-L213, and/or to electrostatically stabilize protons in the interior of the RC.

(1) Paddock, M. L., Rongey, S. H., McPherson, P. H., Feher, G. and Okamura, M. Y. (1994) *Biochem.* 33, 734-745. (2) Takahashi, E. and Wraight, C.A. (1992) *Biochem.* 31, 855-866.
*Work supported by NIH and NSF.

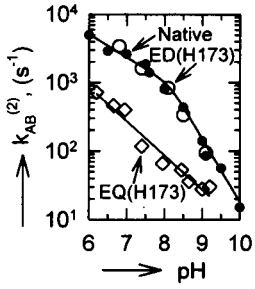


*Fig. Proton-coupled electron transfer ($k_{AB}^{(2)}$) as a function of pH for native, EQ(H173) [Glu-H173 → Gln] and ED(H173) [Glu-H173 → Asp] RCs.*

W-AM-J9

## THE ACID DENATURATION OF PARSLEY PLASTOCYANIN.

((Baifan Li and Elizabeth L. Gross)) Biophysics Program and Biochemistry Department, The Ohio State University, Columbus, OH 43210. (Spon. by E.L.Gross)

Plastocyanin is a 10 KD blue copper protein which functions as a mobile electron carrier shuttling electrons from cytochrome f to P700 in Photosystem I. Since PC is located in the lumen of the thylakoid where it experiences pH value ≤ 5 upon illumination of the chloroplasts, it is very important to study the properties of PC under acid conditions and to examine acid denaturation of PC. The acid denaturation of parsley PC was studied by measuring far-UV CD spectra. The results show that the rate of loss of secondary structure increases as the pH decreases. The log plot of rate of loss of secondary structure vs. pH gives a slope of 2. This indicates that there are two protons involved. The two protons probably are from His residues because of the pH range used in this study. The same result is observed by the monitoring the absorbance of the Cu center at 597 nm. Comparing reduced PC and oxidized PC under the similar pH conditions, the rate of loss the secondary structure for reduced PC is less than for oxidized PC. For instance, at pH 4.66 rate for oxidized PC is 1.74 $hr^{-1}$ and rate for reduced PC is 129.4 $hr^{-1}$. It is concluded that the reduced PC is more stable than the oxidized PC.

# ACTIN

W-AM-K1

## RADIAL COORDINATES OF LOCI IN F-ACTIN.

((C.G. dos Remedios and P.D. Moens)) Muscle Research Unit, Department of Anatomy & Histology, The University of Sydney, Sydney 2006, Australia.

There are three published atomic structures of actin and an atomic structure of chicken breast muscle myosin subfragment-1 (S-1) but to date there is no definitive structure of the atomic structures of actin with S-1. A major impediment to this end has been a degree of uncertainty about the arrangement of actin monomers in F-actin. Holmes et al. (Nature (1990) 347, 44) and Lorenz et al. (J. Mol. Biol. (1993) 234, 826) have suggested a model in which the "large" domain (containing subdomains 3 & 4) is close to the filament axis and the "small" domain (subdomains 1 & 2) are near the filament surface. However, Schutt et al. have proposed a very different arrangement, suggesting that subdomain 2 is nearest the filament axis and subdomain 4 is at the filament surface (Nature (1993) 365, 810). We have attempted to address this problem by examining the radial coordinates of Cys-374, Gln-41 and the tightly-bound nucleotide using fluorescence resonance energy transfer (FRET) spectroscopy. We found it necessary to include phalloidin in the assembly conditions to ensure full and "random" polymerization of the labelled actin monomers and even under these conditions the assembly with some labelled monomers did not assemble randomly. We found the following apparent radial coordinates: 17-18 ± 5 Å for Cys-374; 15-20 ± 5 Å for Gln-41; and (depending on the assumption made) 20 Å for the nucleotide binding site. These coordinates agree well with both the Holmes et al. (27 Å; 24 Å and 20 Å respectively) and with the Schutt et al. (21 Å; 25 Å and 17Å respectively) models but our findings differ somewhat from the published values of Cys-374 and Gln-41.

W-AM-K2

## ISOTROPIC-NEMATIC TRANSITION OF F-ACTIN: A COHERENT PICTURE FROM POLARIZATION MICROSCOPY, RHEOLOGY, CONFOCAL MICROSCOPY, AND ELECTRONMICROSCOPY

((J.X. Tang, J. Käs, and P.A. Janmey)) Brigham and Women's Hospital, Harvard Medical School, LMRC301, Boston, MA 02115.

F-actin forms nematic liquid crystalline phase at a concentration as low as 2 mg/ml, indicating a dynamic persistence length of 10μm. We study the onset concentration of nematic ordering $\rho_l$, as a function of the mean filament length <L>. $\rho_l$ is insensitive to the variation of the filament length as long as <L> is larger than the persistence length. At shorter average lengths of 0.5 to 3μm, we found $\rho_l$ is approximately inversely proportional to <L>. The extreme polydispersity gives rise to a rather wide co-existence region. The co-existing nematic phase, separated from the isotropic phase by low speed centrifugation is 2 to 5 fold more concentrated and contains a higher percentage of longer filaments, detected by electronmicroscopy. Rheology shows an increase of shear modulus with increasing concentration in the isotropic regime. But on the onset of nematic ordering, we observed a distinct decrease of the shear modulus, presumably due to the lower shear resistence of the filaments in the nematic domains that are readily aligned parallel to the shear plates. We have also obtained the first three dimensional images of semiflexible filaments in a nematic phase by confocal microscopy, and followed their dynamics with videomicroscopy. This extends our previous study of F-actin as a model system for semiflexible polymer chains (*Nature*, **368**:226, 1994). In the cell cytoskeletal rim, the liquid crystalline formation is perhaps prevented by actin severing proteins and cross-linking proteins, in order to maintain the mechanical strength of the cell. However, exceptions exist, like in filopodia, where the nematic ordering of F-actin may play a functional role.

**W-AM-K3**

THE STRUCTURAL "FLEXIBILITY" OF ACTIN AS REVEALED IN PROFILIN:ACTIN CRYSTALS. ((J.K. Chik, C.E. Schutt, †R.M. Sweet, and ‡U. Lindberg)) Department of Chemistry, Princeton University, Princeton NJ 08544. †Biology Department, Brookhaven National Laboratories, Upton NY 11973. ‡Department of Zoological Cell Biology, WGI, Arrhenius Laboratories for Natural Sciences, Stockholm University, S-10691 Stockholm, Sweden. (Spon. by Dr. G C. Dismukes)

Recently we reported the crystal structure of the bovine profilin:$\beta$-actin (P:A) complex (Schutt, C.E. *et. al. Nature* **365,** 810–816 (1993)). A complication in structure determination was the sensitivity of the crystal unit cell dimensions to solution conditions (Schutt, C.E. *et. al. J. Mol. Biol.* **209,** 735–746 (1989)). Successful heavy-atom derivatization required an initial transfer of the 1.8M potassium phosphate stabilized crystals into 3.2M $(NH_4)_2SO_4$. This transfer causes the c-dimension to change from 185.7Å to 171.9Å. A 2.65Å data set of the original phosphate crystals was recently collected at the X12C line at NSLS. Using our published $(NH_4)_2SO_4$ stabilized P:A structure, we obtained phases using molecular replacement. Compared to previously published structures, it is evident that significant changes in actin occur whereas profilin appears unchanged. Profilin's apparent structural constancy is consistent with the crystal structure of uncomplexed bovine profilin (Cedergren-Zeppezauer, E.S. *et. al. J. Mol. Biol.* **240,** 459–475 (1994)) which also shows little difference to that found in P:A, except for the n-terminal "switch" region.

**W-AM-K4**

IMAGING OF A COMMON BINDING DOMAIN: ANTI-TnI PEPTIDE MONOCLONAL ANTIBODY MIMICS ACTIN. ((J.E. Van Eyk, R.A. Caday-Malcolm, R.T. Irvin and R.S. Hodges)) Depts. Biochemistry, and Med. Microbiol. Infect. Diseases, Univ. of Alberta, Edmonton, Canada T6G 2H7.

Many multiple-component regulatory systems are controlled by the binding of different receptors to a single common binding domain located on a ligand. The conformation of this common binding domain can be imaged by preparing anti-peptide monoclonal antibodies raised against a synthetic peptide representing a binding site from one of the receptors. These monoclonal antibodies should be able to mimic both the ligand's binding and biological properties. Our goal was to produce an Mab that was able to mimic actin (ligand). Skeletal actin binds to two receptors in a $Ca^{2+}$-dependent manner: troponin I (TnI) and myosin. An actin binding site on TnI is located at the TnI inhibitory region, residues 104-115. Therefore, the 12-residue synthetic peptide of the TnI inhibitory region, was used as a template for the production of a monoclonal antibody (Mab B4). Like actin, the Mab B4 binds to the TnI peptide, native TnI and myosin subfragment 1 (S1). The Mab binding domain on S1 was identified to be amino acid residue 633-644, which has been proposed to be part of an actin-S1 binding interface. In addition, B4 is able to mimic the biological function of actin, and at a 1:1 mole ratio of B4 to S1, B4 induces a 3.6 fold activation of the S1 ATPase activity. This is comparable to F-actin which caused a 4.5 fold activation of the S1 ATPase activity at a 1:1 mole ratio of actin to S1. In a manner similar to the TnI peptide inhibition of the actin-activated S1 ATPase activity, the TnI peptide was able to inhibit the B4-activated S1 ATPase activity. An analog of the TnI peptide containing several semi-conserved changes in the amino acid sequence was unable to inhibit Mab B4 binding to S1 or the B4-activation of the S1 ATPase activity. Therefore, the Mab binds to the inhibitory region of TnI or residues 633-644 of S1 and when bound to S1 induces conformational changes similar to those induced by actin in activating the ATPase activity. Therefore, the anti-TnI peptide Mab is able to mimic actin.

**W-AM-K5**

KINETICS OF THE INTERACTION OF G-ACTIN WITH MYOSIN SUBFRAGMENT-1. EFFECTS OF NUCLEOTIDES AND DNAse I. (( L. Blanchoin*, S. Fievez*, F. Travers**, D. Pantaloni* and M.F. Carlier*))* Laboratoire d'Enzymologie, CNRS, Gif-sur-Yvette and **CNRS, Montpellier, France. (Spon. by M. Le Maire).

The kinetics of interaction of monomeric pyrenyl labelled G-actin with myosin subfragment-1 ($S_1$ ($A_1$) and $S_1(A_2)$ isomers) has been examined in the stopped-flow at low ionic strength. The data confirm the previously reported existence of binary GS and ternary $G_2S$ complexes. The increase in pyrenyl-actin fluorescence which monitors the G-actin-$S_1$ interaction is linked to the isomerization of these complexes following rapid equilibrium binding steps. The rates of isomerization are ~ 200 $s^{-1}$ for GS and ~ 50 $s^{-1}$ for $G_2S$ at 4°C and in the absence of ATP. DNase I and $S_1$ bind G-actin essentially in a mutually exclusive fashion. Both GS and $G_2S$ are dissociated by MgATP and MgADP. However $G_2S$ is much more sensitive to MgATP than GS. The kinetics and mechanism of ATP-induced dissociation of $G_2S$ are quantitatively similar to the ATP-induced dissociation of F-actin-$S_1$, which suggests that $G_2S$ is a good model for the F-actin-$S_1$ interface . The fact that the rates of dissociation of GS and $G_2S$ vary with MgATP in two different fashions also raise the possibility that different mechanical properties of the cross bridge correlate with different orientations of the myosin head and different actin: myosin binding ratios.

**W-AM-K6**

FORCES DEVELOPED BY *DROSOPHILA* WILD-TYPE AND MUTANT ACTIN INTERACTING WITH RABBIT HEAVY MEROMYOSIN MEASURED BY AN OPTICAL TWEEZERS TRANSDUCER ((Molloy, J.E., Burns, J., Sparrow, J.C., & White, D.C.S.)) Department of Biology, University of York, UK

The Figure shows isometric force interactions measured between a single rabbit HMM molecule and (1) rabbit, (2) *Drosophila* flight muscle (DmWT) and (3) mutant *Drosophila* (DmE93K) actin filaments, with an optical tweezers piconewton transducer. The Table summarises the magnitude of (a) the forces under isometric and (b) the displacements under isotonic conditions. Part of the variation in forces may be due to the different distortions between the molecules at the instant of attachment. However, the lower forces produced by the E93K compared to the WT actin are significant.

| Myosin<br>Actin | | HMM<br>**Rabbit** | HMM<br>**DmWT** | HMM<br>**DmE93K** |
|---|---|---|---|---|
| **Force (pN)** | | **1.77** | **1.41** | **0.83** |
| SD | | 0.86 | 0.54 | 0.45 |
| (n) | | (724) | (403) | (50) |
| **Displacement** | | **19.7** | **15.4** | **17.4** |
| SD | (nm) | 7.8 | 6.2 | 4.3 |
| (n) | | (261) | (140) | (41) |

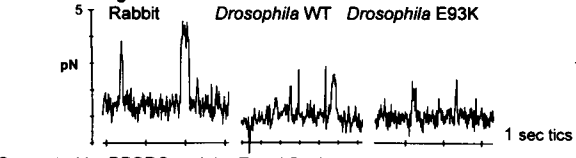


Supported by BBSRC and the Royal Society

**W-AM-K7**

FLEXIBILITY OF ACTIN FILAMENTS DERIVED FROM THERMAL FLUCTUATIONS : EFFECT OF BOUND NUCLEOTIDE, PHALLOIDIN AND REGULATORY PROTEINS. ((H. Isambert*, P. Venier**, A.C. Maggs*, A. Fattoum+, R. Kassab+, D. Pantaloni** and M.F. Carlier**)) *Groupe de Physicochimie théorique, ESPCI, Paris; **Laboratoire d'Enzymologie, CNRS, Gif-sur-Yvette; +CRBM, Montpellier, France.

Single actin filaments undergoing brownian movement in two dimensions were observed at 20°C in fluorescence optical microscopy. The persistence length ($L_p$) was derived from the analysis of either the cosine correlation function or the average transverse fluctuations of series of recorded shapes of filaments assembled from rhodamine-actin. Phalloidin-stabilized filaments had a persistence length of 18± 1 μm, in agreement with recent observations. In the absence of phalloidin, rhodamine-labeled filaments could be observed under a variety of solution conditions once diluted in free unlabeled G-actin at the appropriate critical concentration. Such non stabilized F-ADP-actin filaments had the same $L_p$ of 9 ± 0.5 μm, whether they had been assembled from ATP-G-actin or from ADP-G-actin, and independently of the tightly bound divalent metal ion. In the presence of $BeF_3^-$, which mimicks the γ-phosphate of ATP, F-ADP-$BeF_3$-actin was appreciably more rigid, with Lp = 13.5 μm. Hence newly formed F-ADP-Pi actin filaments are more rigid than "old" F-ADP-actin filaments, which has implications in actin-based motility processes.
In the presence of skeletal tropomyosin and troponin, filaments were rigid (Lp = 20 ± 1 μm) in the off state (-$Ca^{2+}$), and flexible (Lp = 12 μm) in the on state (+ $Ca^{2+}$), consistent with the steric blocking model. In agreement with X-ray diffraction data, no appreciable difference in flexibility was recorded between the off and on states using smooth muscle tropomyosin and caldesmon (Lp = 20 ± 1 μm). In conclusion, this method allows accurate measurement of small (≤ 15%) changes in mechanical properties of actin filaments in correlation with their biological functions.

**W-AM-K8**

THE DYSTROPHIN-GLYCOPROTEIN COMPLEX BINDS F-ACTIN WITH HIGH AFFINITY. ((I.N. Rybakova and J.M. Ervasti)) Department of Physiology, University of Wisconsin Medical School, Madison, WI 53706.

Using a high speed sedimentation assay, it was previously demonstrated that fusion proteins corresponding to the amino-terminal 250 amino acids of skeletal muscle dystrophin bind F-actin in a highly cooperative manner with an apparent $K_d$ of 44 μM (Way et al., *FEBS Lett.* 301: 243, 1992). We previously demonstrated that the purified skeletal muscle dystrophin-glycoprotein complex (DGC) is also capable of cosedimenting with F-actin (Ervasti and Campbell, *J. Cell Biol.* 122: 809, 1993). However, significant binding of DGC to F-actin was observed at an effective dystrophin concentration of 0.1 μM, suggesting that dystrophin in the glycoprotein complex may bind F-actin with significantly higher affinity than synthetic dystrophin fusion proteins. Therefore, the concentration dependence of DGC binding to F-actin was measured using the high speed cosedimentation assay. DGC binding to F-actin saturated near 0.038 mol dystrophin/mol actin, corresponding to one dystrophin per 26 actin monomers. DGC bound to F-actin with an average apparent $K_d$ for dystrophin of 0.4 μM which is similar to the $K_d$ values previously reported for native α-actinin (0.4-0.6 μM). Furthermore, the average Hill coefficient (0.99) calculated from these binding data suggested that dystrophin in the DGC bound F-actin with no cooperativity. We are currently examining whether the dramatic differences between dystrophin amino-terminal fusion proteins and native DGC in F-actin cosedimentation properties are due to an intact dystrophin molecule, dystrophin dimerization or to modulation by other constituents of the DGC or $Ca^{2+}$. Supported by NIH grant (RO1) AR42423 and the Muscular Dystrophy Association.